NACA

RESEARCH MEMORANDUM

EXPERIMENTAL DETERMINATION OF THE SUBSONIC PERFORMANCE OF A RAM-JET UNIT CONTAINING THIN-PLATE BURNERS

By

John R. Henry

Langley Aeronautical Laboratory
Langley Air Force Base, Va.

NATIONAL ADVISORY COMMITTEE
FOR AERONAUTICS

WASHINGTON

June 29, 1949

NACA RM L9B17

NATIONAL ADVISORY COMMITTEE FOR AERONAUTICS

RESEARCH MEMORANDUM

EXPERIMENTAL DETERMINATION OF THE SUBSONIC PERFORMANCE OF A RAM-JET UNIT CONTAINING THIN-PLATE BURNERS

By John R. Henry

SUMMARY

The performance of a ram-jet unit consisting of an intake diffuser, an exhaust nozzle, and a cluster of thin-plate burners contained in a semicircular combustion chamber was investigated in the Langley induction aerodynamics laboratory. Data were taken over a fuel-air-ratio range from 0 to 0.049, a fuel flow range from 0 to 3100 pounds per hour, at combustion-chamber inlet velocities from 40 to 195 feet per second, and at simulated free-stream Mach numbers from 0.20 to 0.55.

Combustion efficiencies from 56 to 72 percent were obtained. At the higher fuel flows investigated, marked decreases in combustion efficiency resulted from increases in fuel flow. This characteristic led to the conclusion that operation under high-thrust-output conditions would not be feasible. It was estimated that the combustion-chamber performance obtained in the subsonic test-stand investigation would produce at supersonic flight speeds thrust coefficients regarded as too low to be practical.

The cycle-efficiency and propulsive-efficiency product of the ram-jet unit was approximately 80 percent of that for a no-pressure-loss unit under the same conditions of operation.

The performance of the intake diffuser, which had an area ratio of 2.14 to 1 and an equivalent conical angle of expansion of 16°, was a unique function of inlet-boundary-layer thickness. Over 99 percent diffuser efficiency was obtained when the boundary layer at the inlet was completely eliminated.

INTRODUCTION

This paper is concerned with the determination of subsonic performance characteristics of the ram-jet burner and combustion-chamber assembly shown in figure 1. The burners and semicircular combustion chamber were designed in 1942 for application as a speed booster to be mounted on the under side

of a fighter airplane. Initial tests were run in the latter part of 1942 in a 3-foot combustion wind tunnel at the Langley Laboratory. To adapt the model to the tunnel a nozzle was placed upstream of the combustion chamber, and to obtain the maximum air flow for the power available the products of combustion were discharged through a diffuser. Due to low tunnel power and lack of instrumentation not many significant quantitative results were obtained; however, crude measurements indicated a 50-percent combustion efficiency at a fuel-air ratio of 0.025 with an inlet velocity of 75 feet per second.

Although rocket developments soon outmoded the speed-booster application of the thin-plate burner, the performance under high-thrust-output conditions was of interest for possible application to supersonic aircraft. When the blower facilities of the Langley induction aerodynamics laboratory became available in 1945, an investigation was initiated to obtain more comprehensive burner performance using a test setup simulating as closely as possible a flight configuration. The simulation consisted of replacing the intake nozzle with an intake diffuser and the exhaust diffuser with an exhaust nozzle and bleeding off the boundary layer at the diffuser inlet. Preliminary tests were run in which the burners were modified to obtain approximately the maximum performance for the present burner configuration. The use of two 1000-horsepower centrifugal blowers and a high-capacity, positive-displacement fuel pump permitted testing over a wide range of fuel and air flows up to back pressures at the diffuser inlet corresponding to a simulated flight Mach number of 0.55. The data have been analyzed in a manner similar to that of reference 1. An estimate, based on the subsonic test-stand data, of thrust coefficients at supersonic flight speeds is presented.

SYMBOLS

The following symbols are used throughout the paper:

A	cross-sectional area, square feet
C_F	thrust coefficient
c_p	specific heat at constant pressure, British thermal units per pound per degree Fahrenheit
F	thrust, pounds
g	acceleration due to gravity, feet per second per second

h_c	lower heating value of fuel (19,000 Btu/lb)
J	mechanical equivalent of heat (778 ft–lb/Btu)
K	friction coefficient
M	Mach number
$\frac{W}{g}$	mass flow, slugs per second
p_t	absolute total pressure, pounds per square foot
p	absolute static pressure, pounds per square foot
p_0	absolute barometric pressure, pounds per square foot
q	dynamic pressure, pounds per square foot
R	gas constant, foot–pounds per pound per degree Fahrenheit
T_t	total temperature, degrees Fahrenheit absolute
T	static temperature, degrees Fahrenheit absolute
V	velocity, feet per second
W_a	air flow, pounds per second
W_f	fuel flow, pounds per second
γ	ratio of specific heat at constant pressure to specific heat at constant volume (considered as variable herein)
δ_0	ratio of absolute barometric pressure to NACA standard atmospheric pressure at sea level, 2116 pounds per square foot absolute $(p_0/2116)$
η	over–all efficiency
η_b	combustion efficiency
η_{tc}	thermodynamic–cycle efficiency
η_d	diffuser efficiency
η_p	propulsive efficiency

[redacted]

θ_{t_5} ratio of absolute total temperature at exhaust-nozzle exit to absolute static temperature at NACA standard atmospheric conditions at sea level, 519° F $\left(T_{t_5}/519\right)$

τ_t ratio of absolute total temperature at exhaust-nozzle exit to absolute total temperature at combustion-chamber inlet $\left(T_{t_5}/T_{t_3}\right)$

F/δ_0 thrust reduced to NACA standard atmospheric conditions at sea level, pounds

$\frac{W_a}{\delta_0}\sqrt{\theta_{t_5}}$ reduced air-flow parameter, pounds per second

$\frac{3600 W_f \eta_b}{\delta_0 \frac{\tau_t - 1}{\tau_t}\sqrt{\theta_{t_5}}}$ reduced fuel-consumption parameter, pounds per hour

Subscripts:

0 to 7 conditions at the corresponding stations indicated in figure 7

x point in any cross section

y point between stations 3 and 4

DESCRIPTION OF APPARATUS

Figure 1 shows the combustion-chamber shell to be a semicircular section suspended from a flat, horizontal structure containing a built-up truss. The $1\frac{7}{32}$-inch space containing the truss served as a cooling shroud for the top of the combustion chamber. The cooling of the curved portion of the combustion-chamber walls was provided for by the addition of a shroud giving a cooling-air passage measuring 1 inch between inner and outer walls. The combustion-chamber length was increased to 5 feet to obtain more complete combustion at the higher fuel flows. The fuel lines were altered so that the individual lines from the burners were manifolded outside of the combustion chamber, instead of inside, in order to simplify maintenance of the setup.

The burners used were modified versions of that shown in figure 2. Fuel was brought into the burners by two lines, the pilot and main feed lines, as shown in figure 2. The pilot fuel traveled through the pilot distributor rake and was projected in 0.024-inch-diameter streams against the interior walls of the upstream region of the pilot housing. The fuel in liquid condition was ignited on and burned from the walls of the pilot housing. The pilot housing created a low-velocity region, necessary for the ignition and existence of the pilot flame. The

main fuel was initially heated by the pilot flame before entering the main boiler. It received further heating in the boiler and then issued from the vapor-jet orifices. The small main vapor jets were ignited by the sheet of flame from the pilot burner and then in turn ignited the large main vapor jets, which had greater penetration. The heat for the main boiler was supplied largely by the burning of the large main vapor jets. A common-rail igniter tube interconnected the five pilot housings so that, if the flame faltered in one housing, ignition would be provided by flame traveling from other pilot housings under the back pressure due to combustion. The small blocking of the thin-plate burner was achieved by the manner of mixing the fuel with the air during the combustion process, which allowed a burner of small frontal area to serve a combustion region of relatively large cross section.

During preliminary runs the pilot burners as shown in figure 2 did not function properly at the higher combustion-chamber inlet velocities. To correct this shortcoming, the pilots were modified as shown in figure 3: the velocity in the pilot housing was reduced by partly closing off the pilot air inlets with drilled rivets and flaring the pilot skirts. The flared skirts probably also induced a certain amount of turbulence in the region of the pilot-housing trailing edge which may have aided the combustion. The modified configuration operated satisfactorily up to full blower capacity with 3100 pounds of fuel per hour and a combustion-chamber inlet velocity of 145 feet per second. Combustion-chamber inlet velocities up to 300 feet per second were obtained by removing the jet discharge nozzle and decreasing the rate of fuel injection in order to reduce the resistance to flow.

The proportions of the diffuser tested are shown diagrammatically in the sketch in figure 4. The configuration of the diffuser exit was determined by the combustion-chamber shape. The inlet shape was made similar to the exit shape except for fillets located in the two upper corners. The diffuser had an equivalent angle of expansion of 16° and a ratio of exit to inlet area of 2.14. The diffuser installation is shown in the photograph of figure 5.

The exhaust-nozzle cross sections were made geometrically similar to that of the combustion-chamber cross section. The nozzle exit area of $1\frac{1}{2}$ square feet was chosen as a result of preliminary calculations to determine that area which would produce the maximum thrust at a fuel-air ratio of 0.03 with the blower air flow and pressure rises available. The nozzle walls were designed to produce an area variation approaching zero at the exit.

The air flow was supplied by two 1000-horsepower centrifugal blowers, series connected, which made available 38,000 cubic feet per minute

[redacted]

at a pressure rise or 150 inches of water. The flow conditions desired at the ram-jet air intake were obtained through use of a fine mesh screen in the low-velocity ducting upstream of the intake, and a boundary-layer bleed gap immediately preceding the intake. A photograph of the ram-jet unit installed in the test cell is presented as figure 6.

The fuel burned in the ram jet was an unleaded 65-octane gasoline. The fuel was pumped through a 30-gallon surge tank, a filter, rotameters, control valves, and the burners. The fuel pressure in the boilers was of the order of 2 to 5 psi gage. The ignition was operated from a 12-volt power source, and a single-electrode 10-millimeter spark plug was used to produce a spark from the center of each pilot housing to the pilot wall.

The instrumentation on the ram-jet unit consisted primarily of pressure tubes and thermocouples, layouts of which are shown in figure 7. In addition to the pressure tubes shown there were three rows of wall static-pressure orifices on the diffuser and a single row along the top of the combustion chamber. All the pressure tubes at station 5 were externally water-cooled. A self-balancing potentiometer accurate to ±1° F was used to read the thermocouple temperatures. All the pressures were made to indicate on a 72-tube manometer board through the use of pneumatically operated pinchboards, and the pressures were photographically recorded. All indicating instruments, controls, and test personnel were housed in a soundproof operating booth.

TESTS

The main program was divided into two series of tests consisting of constant-fuel-flow and variable-blower-speed runs, and vice versa. Each of the series covered the same variable ranges so that a direct cross check was obtained on the reproducibility of the data. The fuel flow range extended from 0 to 3100 pounds per hour, and the blower speed range extended from maximum rotational speed to the lowest rotational speed at which the nozzle-exit gas temperature did not exceed approximately 2400° F. Higher temperatures than 2400° F produced failures in the setup from overheating. The runs lasted about 2 minutes during which fuel flows, temperatures, blower-drive power frequency, and manometer photographic data were recorded. A running record of certain key pressures obtained through the use of airspeed indicators was maintained to insure uniform test results. The ranges of variables covered in the program are listed in the following table.

	Fuel flow (lb/hr)	Combustion-chamber inlet velocity (fps)	Fuel / Air	Free-stream Mach number
Minimum	0	40	0	0.20
Maximum	3100	195	.049	.55

The temperatures and static pressures at the combustion-chamber inlet ranged from 85° F to 125° F and from 2170 to 2600 pounds per square foot absolute, respectively.

COMPUTATION METHODS

A diagrammatic sketch of the simulated ram-jet configuration is presented in figure 7. Stations 0 and 7 are by definition stations at which the static pressure is equal to the free-stream static pressure; adiabatic flow was assumed between stations 0 and 1 and between stations 5 and 7. In order to calculate the parameters presented in this paper it was necessary to determine almost all quantities identifying the flow at all stations except station 4. The methods used in obtaining these quantities are outlined in the following paragraphs.

The static-pressure variations at stations 2, 5, and 6 and the total-temperature variations at stations 2 and 6 were so small that arithmetic averages of the data reading could be used. An exact determination of the average total pressure at station 5 would have required knowledge of both total-pressure and temperature variations across the section. Data from preliminary tests in which thermocouple measurements were taken at station 5 were used to obtain an indication of the order of magnitude of the discrepancies between arithmetic and weighted averages of $(p_{t_5} - p_0)$. The arithmetic average differed from the weighted by less than 5 percent for all cases. These inaccuracies were not considered of sufficient magnitude to justify the added work of data reduction and complication in instrumentation necessary to measure temperatures, especially in view of the irregularity of the total-pressure gradients, examples of which are presented in figure 8. Therefore, the average total pressure at station 5 was obtained by arithmetic averages of the tube readings. The static pressure at station 1 was determined through the use of a calibration of the three static-tube readings taken at station 1. The calibration was obtained by surveying the static pressure at the station over a range of air flows for several resistances to flow obtained by installing

[redacted]

screens on the nozzle exit. The total pressure at station 1 was constant across the section except for a negligible area adjacent to the wall.

The total-pressure readings from the two rakes at station 6 (see fig. 7) were used to determine a ratio of the weighted average total pressure to the center of the passage total pressure. The average total pressure at the shroud exit was taken to be the product of this ratio and the arithmetic average of the center of the passage tube readings. Average measured pressures and temperatures were plotted against fuel flow and percent of maximum blower speed. All calculations were made using faired values from these curves, examples of which are presented in figures 9 and 10. Figure 9(a) shows average measured diffuser-exit static pressures taken from runs made with constant fuel flow and varying blower speed. Similar data taken at constant blower speed and variable fuel flow are shown in figure 9(b), which also shows solid points taken from faired curves of figure 9(a). The agreement between the curves and the solid points indicates the relative value of faired data obtained by the two methods. Similar data and comparisons are given for nozzle-exit total pressure in figures 10(a) and 10(b).

The following are relations used in the computations:

Velocity

$$V = \sqrt{\frac{2\gamma g R T_t}{(\gamma - 1)}\left[1 - \left(\frac{p}{p_t}\right)^{\frac{\gamma-1}{\gamma}}\right]}$$

Mass flow at stations 1 and 6

$$\frac{W}{g} = A_p\sqrt{\frac{2\gamma}{gR(\gamma - 1)T_t}\left(\frac{p_t}{p}\right)^{\frac{\gamma-1}{\gamma}}\left[\left(\frac{p_t}{p}\right)^{\frac{\gamma-1}{\gamma}} - 1\right]}$$

Dynamic pressure at stations 2 and 3

$$(p_t - p) = p\left\{\left[\frac{1}{2} + \sqrt{\frac{gRT_t(\gamma - 1)}{2\gamma p^2}\left(\frac{W}{gA}\right)^2 + \frac{1}{4}}\right]^{\frac{\gamma}{\gamma-1}} - 1\right\}$$

[redacted]

Total temperature at station 5

$$T_{t_5} = \frac{2\gamma}{gR(\gamma - 1)} \frac{p_5^2}{\left(\frac{W_5}{g}/A_5\right)^2} \left[\left(\frac{p_{t_5}}{p_5} \right)^{\frac{\gamma-1}{\gamma}} - 1 \right] \left(\frac{p_{t_5}}{p_5} \right)^{\frac{\gamma-1}{\gamma}}$$

Mach number at station 0

$$M_0 = \sqrt{\frac{2}{\gamma - 1} \left[\left(\frac{p_{t_0}}{p_0} \right)^{\frac{\gamma-1}{\gamma}} - 1 \right]}$$

RESULTS AND DISCUSSION

Ram-jet performance can be expressed in many different terms according to what purpose is being accomplished. The thrust force is a significant quantity that can be directly compared with the drag force of the body to determine the resulting equilibrium level-flight speed or the possible acceleration at a given flight speed and rate of climb. Thrust is often more usefully thought of in terms of a dimensionless coefficient C_F, which is comparable to the drag coefficient of a body. Neither of these quantities reflects fuel economy or efficiency of energy conversion. Over-all efficiency is the product of burner, thermodynamic-cycle, and propulsive efficiencies and expresses the percentage of energy in the fuel converted to thrust energy. The reciprocal of the over-all efficiency is proportional to the specific fuel consumption and indicates the fuel rate required per unit thrust horsepower.

An analysis of the relation of ram-jet performance parameters to flight Mach number is given in reference 1. Performance curves similar to those of reference 1 have been prepared from the data taken on the thin-plate-burner ram-jet configuration. A plot of reduced thrust (thrust/δ_0) against simulated flight Mach number is presented in figure 11. Thrust was calculated using the following equation:

$$F = \frac{W_3}{g}(V_7 - V_0)$$

It is estimated that the thrust values shown in figure 11 are accurate to ±10 percent. An analysis of figure 11 shows that for a given temperature ratio the reduced thrust is proportional to the simulated flight Mach number to a power which varies between 1.8 and 2.1. The highest thrust attained in the tests was 410 pounds at a Mach number of 0.54 and a temperature ratio τ_t of 3.0.

[redacted]

The relation of thrust coefficient C_F to simulated flight Mach number is presented in figure 12. Thrust coefficient was defined as follows:

$$C_F = \frac{F}{q_0 A_3} \tag{1}$$

The area A_3 was used as the reference area because the cooling shroud would not necessarily be used in a flight model. Thrust coefficients from 0.370 to 0.397 were attained at a temperature ratio of 5.0. Figure 12 indicates that within the accuracy of the data the ram-jet unit produced no variation of C_F in the Mach number range covered by the tests for constant temperature ratio τ_t.

The range of simulated flight Mach number obtained in the test was limited and the relation of the low Mach number data to possible high Mach number performance was not obvious; therefore, an estimate based on the subsonic test-stand data was made of the thrust-coefficient variation with flight Mach number. The combustion-chamber performance in terms of Mach numbers and pressure and temperature ratios was held to those values obtained in the tests regardless of the flight Mach number. It was believed reasonable to restrict the combustion-chamber inlet velocity by limiting the inlet Mach number to test values since most ram-jet burners depreciate in performance if the air velocity is increased beyond certain values. This limitation would be imposed physically by regulation of the nozzle exit area. The limitation of the combustion-chamber temperature ratios to test values is considered conservative since the higher levels of pressures and temperatures associated with higher flight Mach numbers are favorable to combustion. Further discussion of the assumptions and methods used in the calculations is given in the appendix.

Two cases were calculated, one for a temperature-rise ratio of 3.85 and a combustion-chamber inlet Mach number of 0.065 (fig. 13) and one for a temperature-rise ratio of 2.89 and an inlet Mach number of 0.085 (fig. 14). For inlet-total-pressure-recovery ratios of 80 and 90 percent both figures 13 and 14 show a continuously rising thrust coefficient with flight Mach number; however, for 100-percent inlet-total-pressure-recovery ratio both cases show a peak thrust coefficient in the region of a flight Mach number of 0.25 to 0.40 and a minimum thrust coefficient in the region of a flight Mach number of 1.0 to 1.4.

In discussing the calculated curves comparisons will be drawn with the test-data curves of figure 12, which differ significantly from the calculated curves in that the test-data curves are for a variable instead of a constant combustion-chamber inlet Mach number and a constant instead

of a variable nozzle exit area. Only one point from either figure 13 or 14 corresponds in every respect with a group of conditions on the test-data plot. Such a point common to figures 12 and 13 occurs at a thrust coefficient of 0.367 and a flight Mach number of 0.375. This point has a total-pressure-recovery ratio of 99.5 percent, a total-temperature ratio of 4.75, a combustion-chamber inlet Mach number of 0.065, and a nozzle exit area equal to that of the test setup.

Moving, in figure 13, from this common point to lower flight Mach numbers along a 99.5-total-pressure-recovery-ratio curve results in higher thrust coefficients, whereas in figure 12 on the 4.75-temperature-ratio curve the same procedure results in almost the same thrust coefficient. Higher thrust coefficients are obtained along the 99.5-total-pressure-recovery-ratio curve because the inlet Mach number and therefore the air flow are held constant by opening up the nozzle exit, but in the test-data curves the rate of thrust-coefficient increase is less because the nozzle exit is held constant and the inlet Mach number of air mass flow is allowed to decrease. However, continued movement to lower flight Mach numbers along the 99.5-pressure-recovery curve leads to a condition where relatively high internal losses due to maintenance of approximately a constant air flow, a large nozzle exit area, and low ram pressures combine to reduce the exit velocity to the same order of magnitude as the flight velocity, and the thrust coefficient approaches zero rapidly. This situation never occurs in the constant-nozzle-exit-area case (fig. 12) because the inlet Mach number is allowed to decrease and the internal losses stay more in proportion to the decreasing ram pressures. Movement from the common point to higher flight Mach numbers invokes arguments converse to those for movement in the opposite direction. The higher rate of decrease in thrust coefficient of the 99.5-pressure-recovery curve with respect to the 4.75-temperature-ratio curve of figure 12 is principally due to the limitation of the air flow in figure 13 caused by the decreasing nozzle exit area as compared to the constant nozzle exit area and increasing air flow of figure 12.

The final rise in thrust coefficient of the curves of figures 13 and 14 is due to the thrust coefficient being referenced to flight dynamic pressure instead of flight stagnation-pressure rise, as is evident from the dashed curve of figure 13.

The thrust coefficients shown in figures 13 and 14 for the supersonic flight range are regarded as too low to be of practical value. The possibility of increasing the thrust coefficient by increasing the inlet Mach number or air flow and/or the temperature rise will be shown in a later discussion to be remote. Therefore, it appears that the thin-plate burner does not have direct application to supersonic aircraft.

For a given altitude, flight Mach number, burner efficiency, and temperature ratio τ_t, it is possible to determine from figures 15 and 16 the air flow and fuel flow required to obtain a given thrust condition chosen from figure 12. Figure 15 is a plot of the air-flow parameter against simulated flight Mach number, for constant values of temperature ratio τ_t. The parameter includes the quantity θ_{t_5}, which can be determined from the temperature ratio τ_t, the flight Mach number, and the altitude. The maximum deviation of the data from the curves was less than 1 percent on the basis of curves of constant temperature ratio. The air-flow parameter $\frac{W_a}{\delta_0}\sqrt{\theta_{t_5}}$ for a ram-jet unit with a hypothetical combustion chamber of zero pressure losses, is not a function of the temperature ratio (see reference 1), but for an actual unit with appreciable combustion-chamber gas velocities the momentum pressure losses increase with increasing values of temperature ratio, and it is necessary to take into account variations in temperature ratio in correlating the air-flow requirements.

Figure 16 is a plot of the fuel-flow parameter against simulated flight Mach number. This parameter includes the burner efficiency, which must either be determined or assumed in order to make use of the curve. The parameter differs from the one of reference 1 in that the temperature ratio τ_t is included to correct for the combustion-chamber losses. With the inclusion of this term the maximum scatter of the data was ± 2 percent.

The over-all efficiency was calculated from

$$\eta = \frac{FV_0}{W_f h_c J}$$

This is the ratio of the thrust power to the combustion energy in the fuel and can be shown to be the product of the burner, cycle, and propulsive efficiencies. The ratio of the heat received by the air to the heat of combustion of the gas is the combustion efficiency,

$$\eta_b = \frac{(W_a + W_f) c_{p_{3-5}} (T_{t_5} - T_{t_3})}{W_f h_c}$$

The ratio of the over-all efficiency to the burner efficiency is equal to the product of the cycle and propulsive efficiencies and can be considered as the efficiency with which the heat received by the air is converted to thrust power.

[redacted]

The cycle efficiency for a hypothetical ram jet with no pressure losses is given in equation (10) of reference 2 as

$$\eta_{tc} = \frac{1}{1 + \frac{2}{(\gamma - 1)M_0^2}}$$

The actual propulsive efficiency is given in equation (20) of reference 2 as

$$\eta_p = \frac{1}{1 + \frac{1}{2}\left(\frac{V_7 - V_0}{V_0}\right)}$$

The last expression for a ram jet with no pressure losses reduces to

$$\eta_p = \frac{2}{1 + \sqrt{\tau_t}}$$

The over-all efficiency for a ram jet with no pressure losses is therefore a function of three variables: burner efficiency, flight Mach number, and temperature ratio.

The product of the actual cycle and propulsive efficiencies (as obtained by dividing the over-all efficiency by combustion efficiency) is plotted against simulated flight Mach number in figure 17 for several temperature ratios. A value of 3.6 percent was reached with a temperature ratio of 3 at a simulated flight Mach number of 0.545 which corresponded in this case to an over-all efficiency of 2.04 percent.

The ratio of the actual cycle-efficiency and propulsive-efficiency product to the product of the cycle and propulsive efficiencies for a no-loss system is plotted against the simulated flight Mach number in figure 18. No reliable trends are indicated by the data but the order of magnitude of the ordinate is 0.80. In this comparison the burner efficiency is not a factor and the 20-percent drop below 100 percent must be charged to internal friction, turbulence losses, and momentum-pressure losses occurring in the diffuser and combustion chamber.

In order to determine the contribution to this loss chargeable to diffuser losses, pressure measurements were made to determine the diffuser efficiency

[redacted]

$$\eta_d = \frac{\Delta p_{1-2}}{\left(p_{t_1} - p_1\right) - \left(p_{t_2} - p_2\right)}$$

A plot of these values against the air-bleed pressure coefficient gave the curve of figure 19 with a point scatter of ±1 percent-units. The points in figure 19 were from runs with no combustion using screen resistances. It is apparent that the diffuser efficiency is a function of the pressure and mass-flow conditions at the bleed and is not affected by combustion as such. The low-pressure-coefficient end of the curve, which drops below 99 percent efficiency, is for very lean mixtures (fuel-air ratios of 0.022 or less) so that most of the combustion data were taken with a diffuser efficiency of 99 percent. The high efficiency is due to complete removal of the boundary layer at the diffuser inlet, thus preventing the occurrence of boundary layers of sufficient thickness to separate within the diffuser length. It can be concluded that the 20-percent drop below the ideal efficiency must be charged almost entirely to combustion-chamber momentum, friction, and turbulence losses.

The combustion efficiency is a function of many variables including the type of burner, the combustion-chamber configuration, the pressure and temperature of the intake air, the fuel and air distribution, the fuel flow, the combustion-chamber inlet-air velocity, the fuel-air ratio, and the type of fuel. The fuel flow and air flow (and consequently the combustion-chamber inlet velocity and fuel-air ratio) were the principal variables in the test program. The relation of the measured combustion efficiency to these variables is illustrated by figure 20, which is a family of curves of constant combustion efficiency plotted on coordinates of fuel and air flows. Superimposed on the principal coordinates are curves of constant combustion-chamber inlet velocity, temperature rise through the combustion chamber, and fuel-air ratio. All the variables plotted in figure 20 are interrelated; however, it is possible to draw some general conclusions concerning the combustion efficiency. It is apparent from the efficiency curves that the lean-mixture tests were not extended to high enough combustion-chamber inlet velocities to obtain marked decreases in combustion efficiency due to approaching the blow-out condition. This effect would have caused a decreasing negative slope of the lower-value efficiency curves with increasing air flow at constant fuel flow.

It is also apparent that it was somewhat more efficient to burn a given quantity of fuel at high fuel-air ratios or low air flows. It is difficult to deduce the reason for this effect; it is possible that

the hotter pilot flame at the lower air flows improved the evaporation and ignition of the main boiler fuel, and it is also possible that the lower air flows allowed the main boiler fuel jets to penetrate further into the air stream producing a more homogeneous mixture. Burning a given amount of fuel at low air flows also means burning at high combustion temperatures, as is indicated in figure 20. It is possible that this process was more efficient because of the beneficial effect of high temperature on combustion.

The variable which affected the efficiency to the greatest degree is shown by figure 20 to be the fuel flow, especially at the highest air flows. There may have been some loss in efficiency with increasing fuel flows due to exceeding the evaporative capacity of the boilers although this effect should have been minimized because the pilot fuel flow was increased proportionally with the main-boiler fuel flow. There undoubtedly is a change in fuel, fuel-air, and air distributions with increasing fuel flow at constant air flow. A locally enriched burning mixture should create an increased local resistance to air flow thus enriching the mixture further until a static pressure equilibrium with the surrounding air stream is reached. If the local region is at stoichiometric mixture before the enrichment takes place, the excess fuel may never burn with air from the surrounding regions and thus the over-all combustion efficiency drops. It is believed that such phenomena took place in the region of each of the five burners, causing five retarded regions surrounded by regions of high mass flow rates. At station 5 thermocouple and pressure measurements taken in preliminary tests indicated that the combustion had spread between the five regions forming a central core of hot gases surrounded by a relatively cool annulus of high mass flow rate adjacent to the wall. These phenomena were substantiated by visual observation.

Because the thin-plate-burner configuration has the characteristic of decreasing combustion efficiency with increasing fuel flow, it is quite evident that operation under high-thrust-output conditions, for instance a fuel-air of 0.06 and a combustion-chamber inlet velocity of 150 feet per second, is not feasible.

It is possible that longer combustion chambers might have provided better mixing and more complete combustion. This is substantiated in figure 21 by the slope of the curves of static pressure along the combustion chamber. The curves indicate that for the higher fuel flows combustion was still proceeding at the end of the combustion chamber, whereas for the lowest fuel flow shown the slope of the curve near the end of the combustion chamber is of the same order of magnitude as that which would result from the friction pressure drop alone.

[redacted]

CONCLUDING REMARKS

The thin-plate-burner configuration produced combustion efficiencies ranging between 56 and 72 percent in the ranges of variables covered by the tests. At the higher test fuel flows the burners exhibited marked decreases in efficiency with increasing fuel flows, which is believed to be caused by increasing maldistribution with increasing fuel flows. Because of this characteristic, operation of the thin-plate-burner configuration under high-thrust-output conditions is not considered feasible.

The ram-jet unit produced approximately constant thrust coefficients with variation of simulated flight Mach number for curves of constant combustion-chamber total-temperature ratio, variable combustion-chamber inlet Mach number, and constant nozzle exit area. Estimates of thrust coefficients at supersonic flight speeds for combustion-chamber performances limited to those obtained in the tests produced values regarded as too low to be practical.

The cycle-efficiency and propulsive-efficiency product of the ram-jet unit was approximately 80 percent of that for a no-pressure-loss unit under the same conditions of operation.

The performance of the intake diffuser, which had an area ratio of 2.14 to 1 and an equivalent conical angle of expansion of 16° was a unique function of the inlet-boundary-layer thickness. Over 99-percent diffuser efficiency was obtained when the boundary layer at the inlet was completely eliminated.

Langley Aeronautical Laboratory
National Advisory Committee for Aeronautics
Langley Air Force Base, Va.

[redacted]

APPENDIX

ESTIMATION OF THRUST COEFFICIENTS FOR SUPERSONIC FLIGHT SPEEDS

The range of simulated flight Mach number obtained in the tests was limited and the relation of the low Mach number data to possible high Mach number performance was not obvious; therefore, an estimate based on the subsonic test-stand data was made of the thrust-coefficient variation with flight Mach number. The combustion-chamber performance in terms of Mach numbers and pressure and temperature ratios was held to those values obtained in the test regardless of the flight Mach number. It was believed reasonable to restrict the combustion-chamber inlet velocity by limiting the inlet Mach number to test values since most ram-jet burners depreciate in performance if the air velocity is increased beyond certain values. This limitation would be imposed physically by regulation of the nozzle exit area. The limitation of the combustion-chamber temperature ratios to test values is considered conservative since the higher levels of pressures and temperatures associated with higher flight Mach numbers are favorable to combustion. It was further assumed that the friction and turbulence loss characteristics of the combustion chamber remained unchanged.

In attempting to derive expressions relating the temperatures and pressures before and after combustion in a tube of constant cross-sectional area the problem arises as to how to account for friction and turbulence losses. Actually friction and turbulence losses occur along the entire length of the chamber, the amount of loss over any one section depending on the chamber and burner design. To attempt to write such an exact friction loss distribution into combustion equations would be extremely difficult. For the purpose of this presentation it will be assumed that the over-all loss can be represented in two parts, the first part being proportional to the dynamic pressure before combustion and the second part expressed as being proportional to the dynamic pressure after combustion, thus the sum of K_3q_3 and K_4q_4 is equal to the total loss. On this basis the following expressions can be written:

$$\frac{p_4}{p_3} = \frac{\gamma_3\left[1 + \gamma_3\left(1 - \frac{K_3}{2}\right)M_3^2\right]}{\gamma_4\left[\frac{\gamma_3}{\gamma_4} + \gamma_3\left(1 + \frac{K_4}{2}\right)M_4^2\right]} \tag{A1}$$

$$\frac{p_{t_4}}{p_{t_3}} = \frac{p_4}{p_3}\frac{\left(1 + \frac{\gamma_4 - 1}{2}M_4^2\right)^{\frac{\gamma_4}{\gamma_4 - 1}}}{\left(1 + \frac{\gamma_3 - 1}{2}M_3^2\right)^{\frac{\gamma_3}{\gamma_3 - 1}}} \tag{A2}$$

$$\frac{T_{t_4}}{T_{t_3}} = \frac{\gamma_4}{\gamma_3}\left(\frac{p_4}{p_3}\right)^2 \frac{R_3}{R_4}\frac{M_4^2}{M_3^2}\frac{\left(1 + \frac{\gamma_4 - 1}{2}M_4^2\right)}{\left(1 + \frac{\gamma_3 - 1}{2}M_3^2\right)} \tag{A3}$$

An inspection of the equations reveals that a simultaneous solution is possible which expresses the total-pressure ratio as a function of Mach number before combustion, total-temperature ratio, friction coefficients, specific heats, and gas constants. Also, through use of equations (A1) and (A2) it is possible to express total-pressure ratio as a function of Mach numbers before and after combustion, friction coefficients, and specific heats. Figure 22 illustrates these functions for standard air values of the ratio of specific heats and the gas constant and approximately the value of friction loss and distribution corresponding to the test ram-jet combustion chamber. The plot assumes that the friction-loss coefficients remain constant for all conditions of combustion-chamber operation. A test-data plot, similar to that of figure 22, is presented in figure 23, which was used to determine the total-pressure ratio across the combustion chamber in the supersonic thrust-coefficient calculations. A comparison of the hypothetical combustion-chamber characteristics and the actual characteristics is made in figure 24. An inspection of the figure reveals that a closer comparison probably could have been attained by choosing a hypothetical combustion chamber with a slightly lower friction-loss coefficient concentrated more heavily at the combustion-chamber outlet.

[redacted]

Using equation (1), figure 23 and standard air values of specific heats and the gas constant, thrust coefficients were calculated for assumed values of flight Mach number, combustion-chamber inlet Mach number and total-temperature-rise ratio, and diffuser total-pressure-recovery ratio. Figures 25, 26, 27, and 28 present calculated curves of constant thrust coefficient plotted on ordinates of total-temperature-rise ratio and inlet Mach number for flight Mach numbers of 1.0 and 2.0 with diffuser total-pressure-recovery ratios of 80 and 100 percent. The curves indicate that the highest supersonic flight thrust coefficients are obtained at the test-data boundary which extends from high temperature-rise ratios and moderate inlet Mach numbers to high inlet Mach numbers and moderate temperature-rise ratios. Therefore, in order to indicate the variation with flight Mach number of approximately the maximum thrust coefficient, two conditions along this boundary of inlet Mach number and temperature-rise ratio were chosen. This variation is illustrated in figures 13 and 14 and is discussed under the section "Results and Discussion."

[redacted]

REFERENCES

1. Perchonok, Eugene, Wilcox, Fred A., and Sterbentz, William H.: Preliminary Development and Performance Investigation of a 20-Inch Steady-Flow Ram Jet. NACA ACR No. E6D05, 1946.

2. Rubert, Kennedy F.: An Analysis of Jet-Propulsion Systems Making Direct Use of the Working Substance of a Thermodynamic Cycle. NACA ACR No. L5A30a, 1945.

[redacted]

NACA – Digidocs

Document processing error

Unreadable tiff image

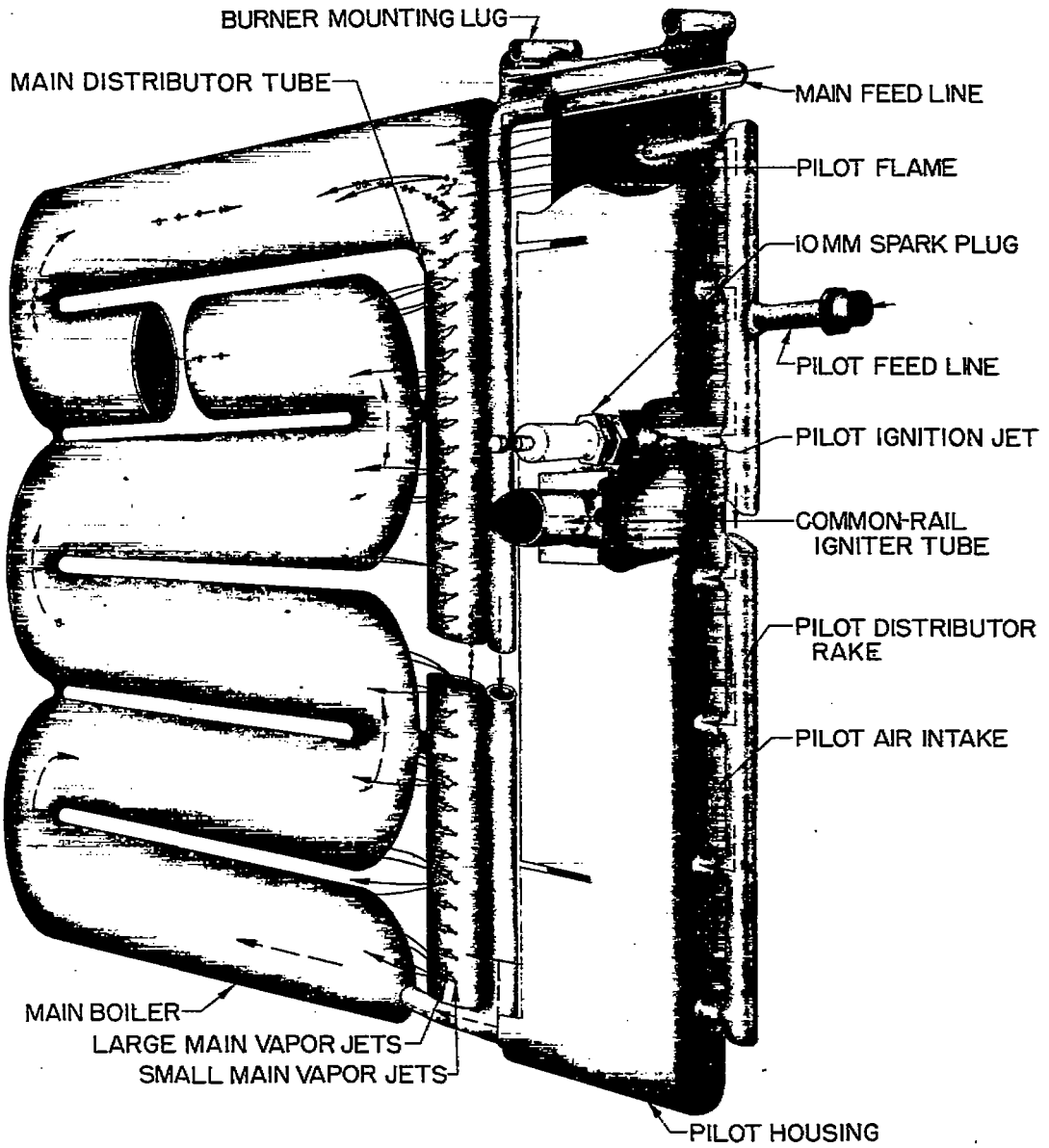

Figure 2.- Thin-plate-burner unit with nonvaporizing pilot burner.

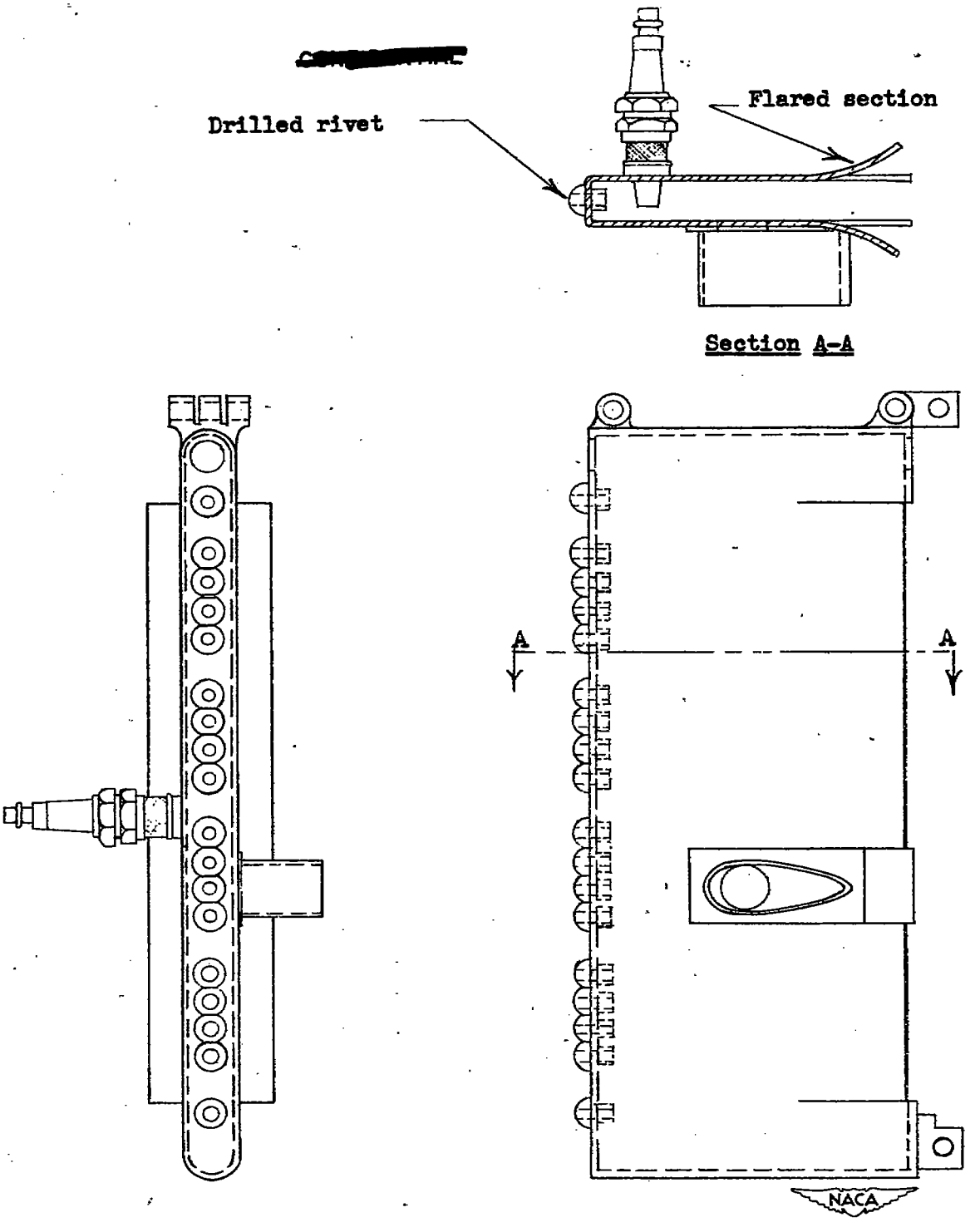

Figure 3.– Modified nonvaporizing pilot-burner housing.

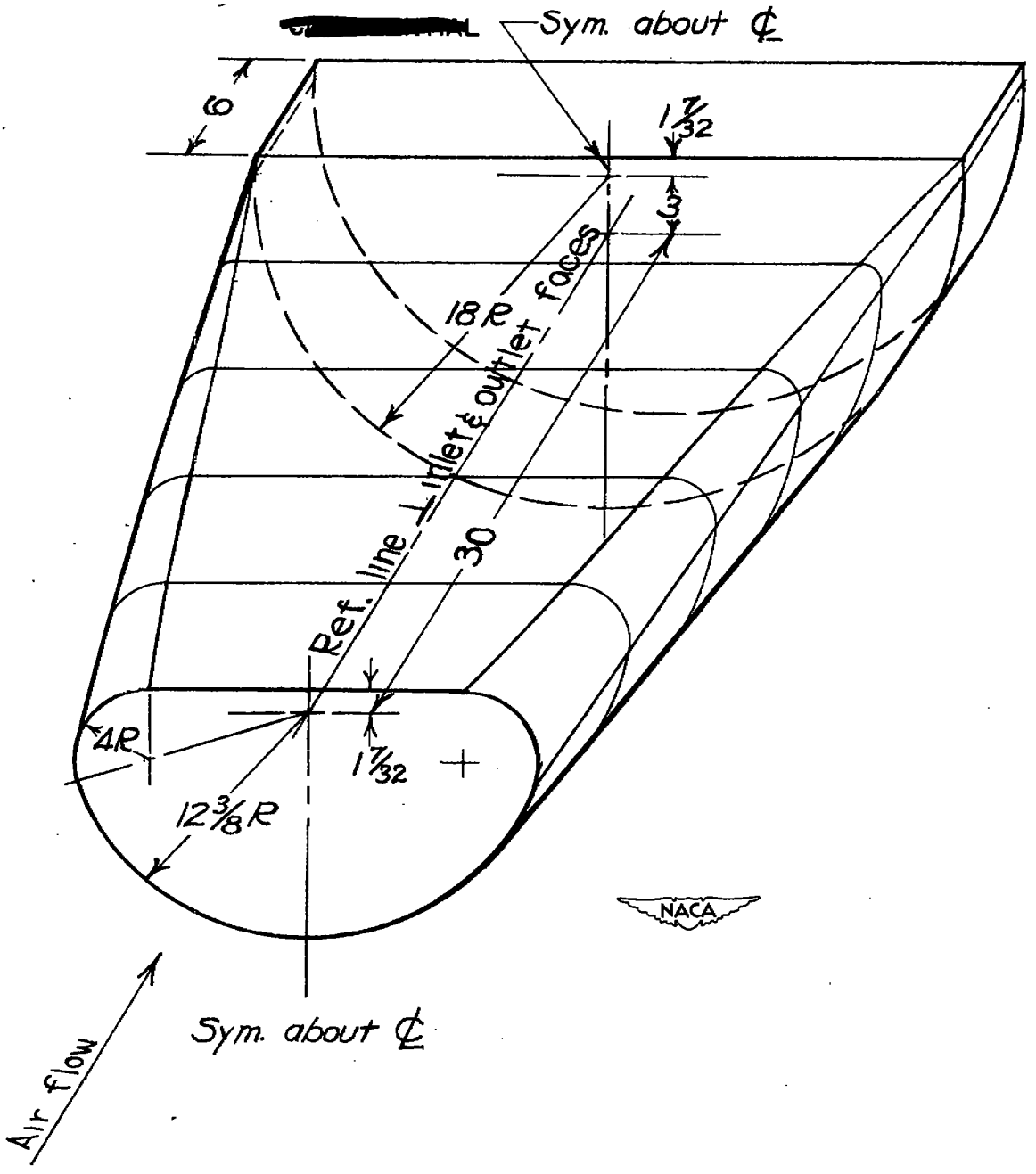

Figure 4.– Diagrammatic sketch of inlet diffuser.

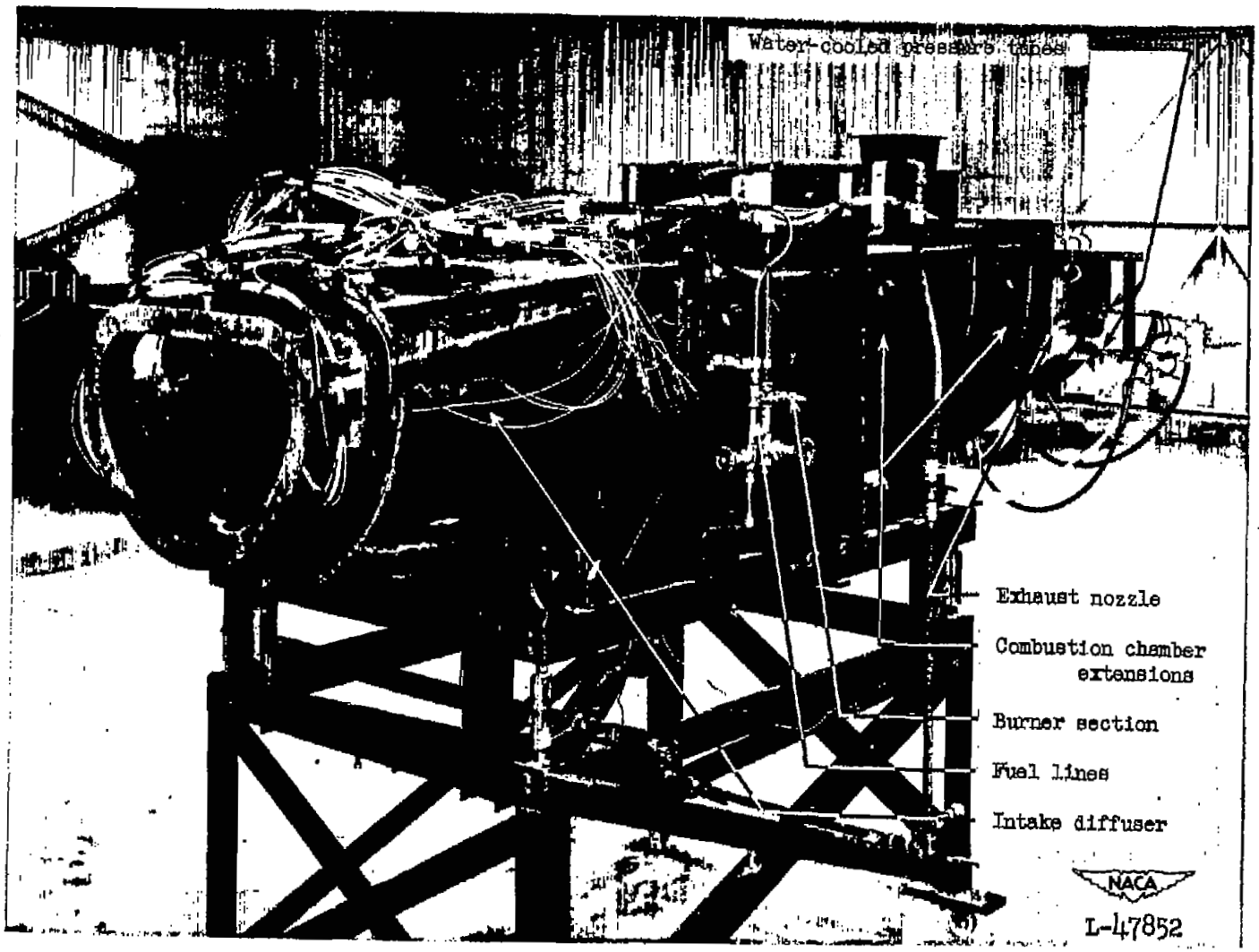

Figure 5.- Experimental setup.

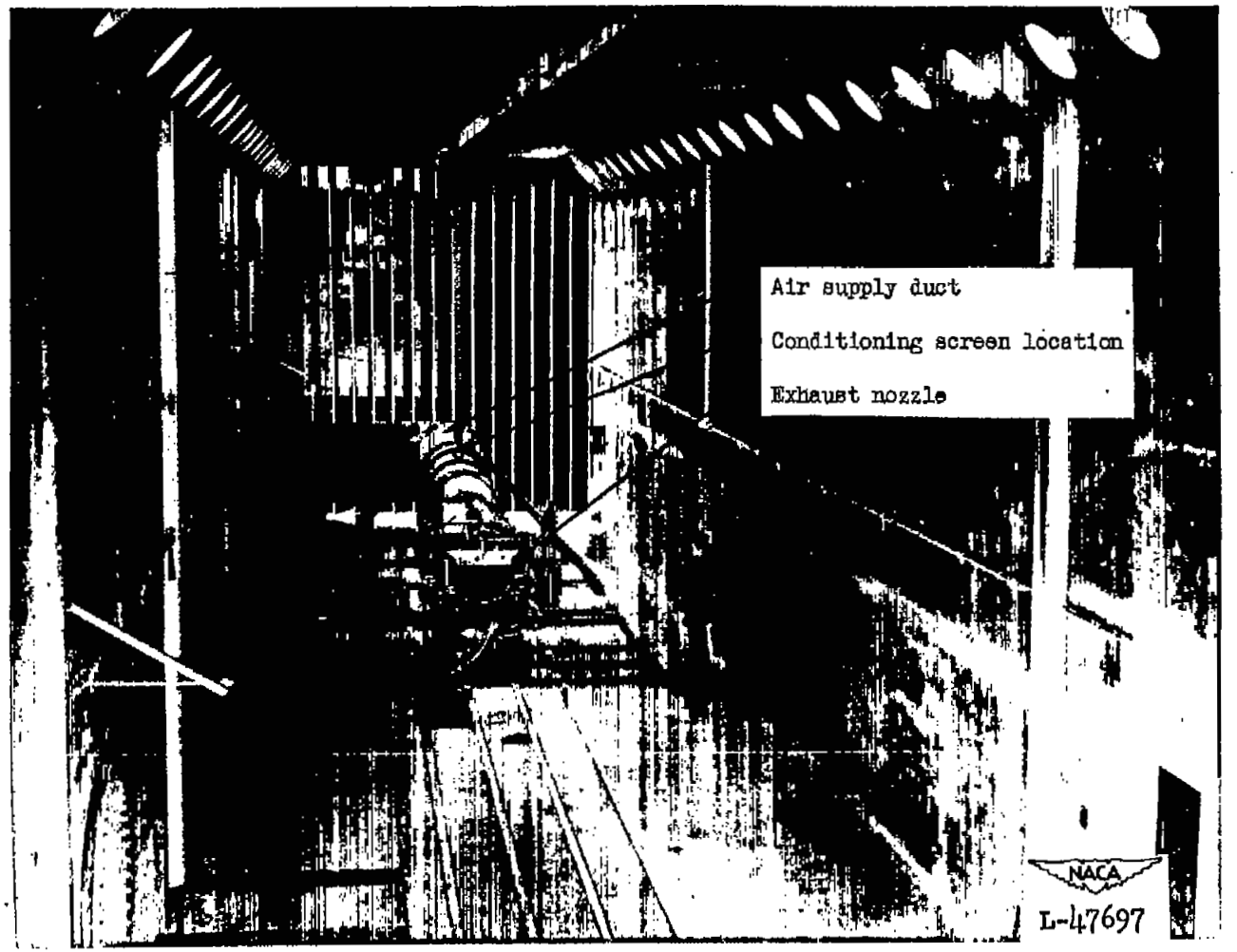

Figure 6.- View from test-cell exit of ram-jet test installation.

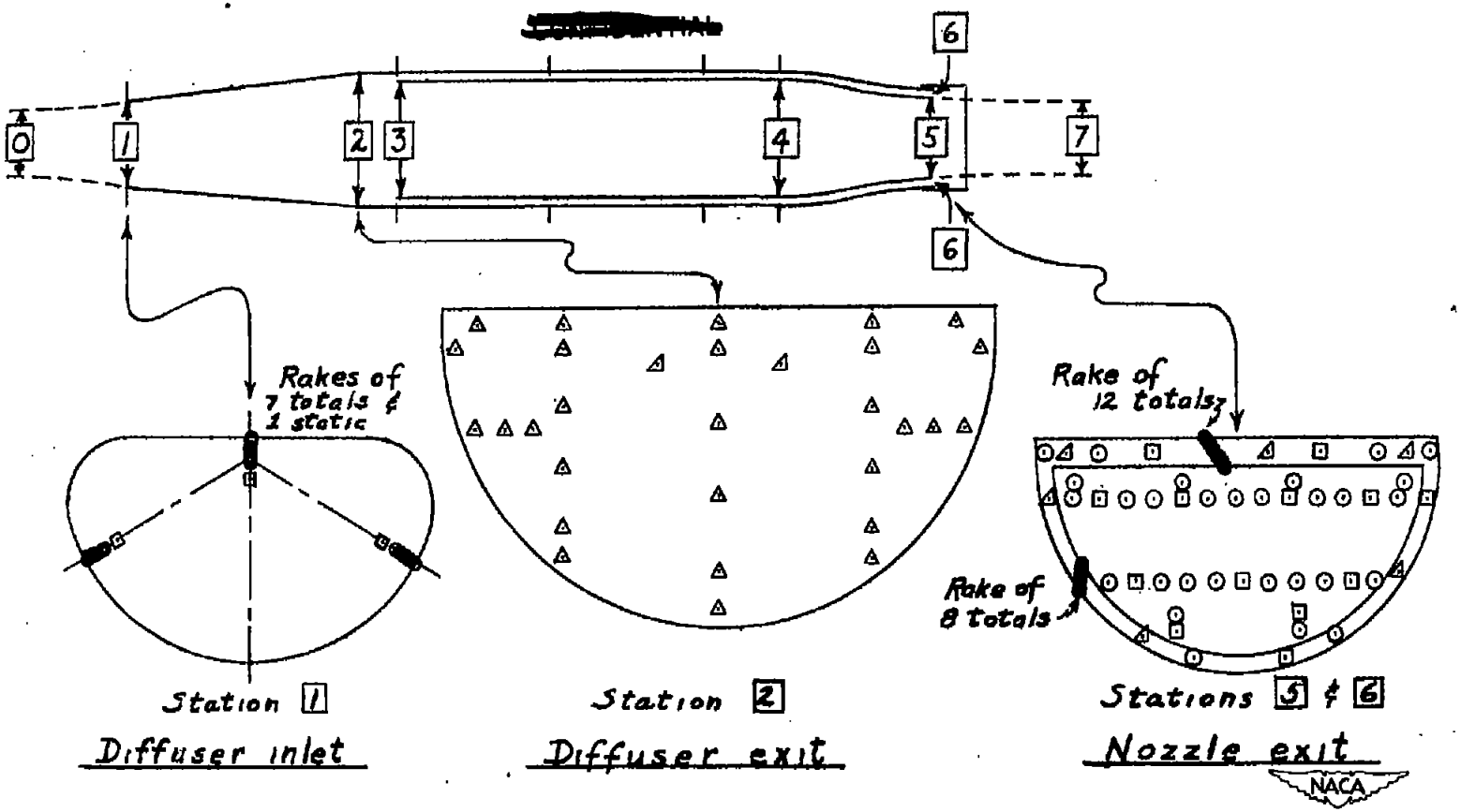

Figure 7.– Sketch of ram-jet unit showing pressure-tube layouts and reference stations.

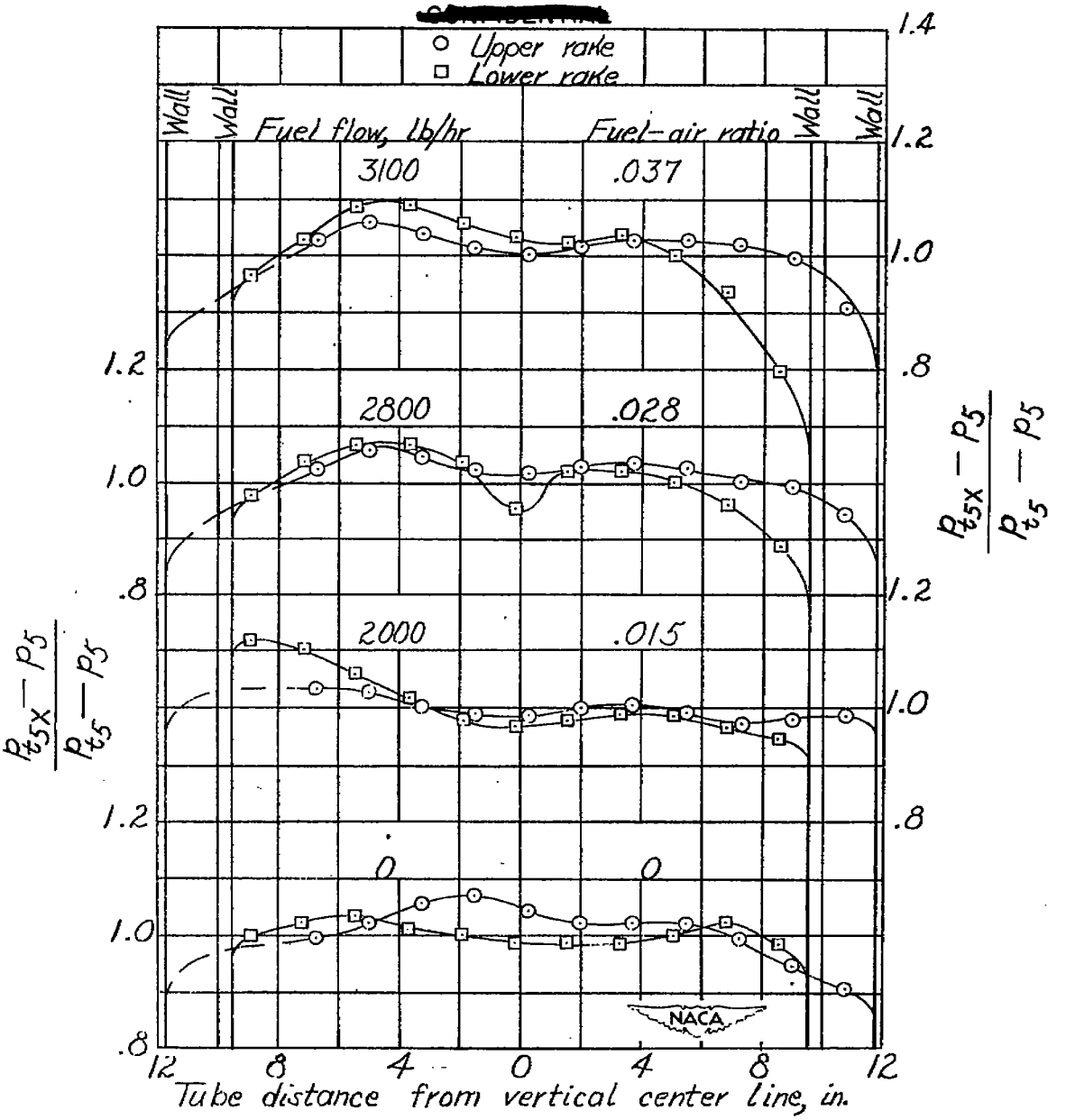

Figure 8.– Horizontal dynamic-pressure gradients from rake readings at station 5. (See fig. 7.)

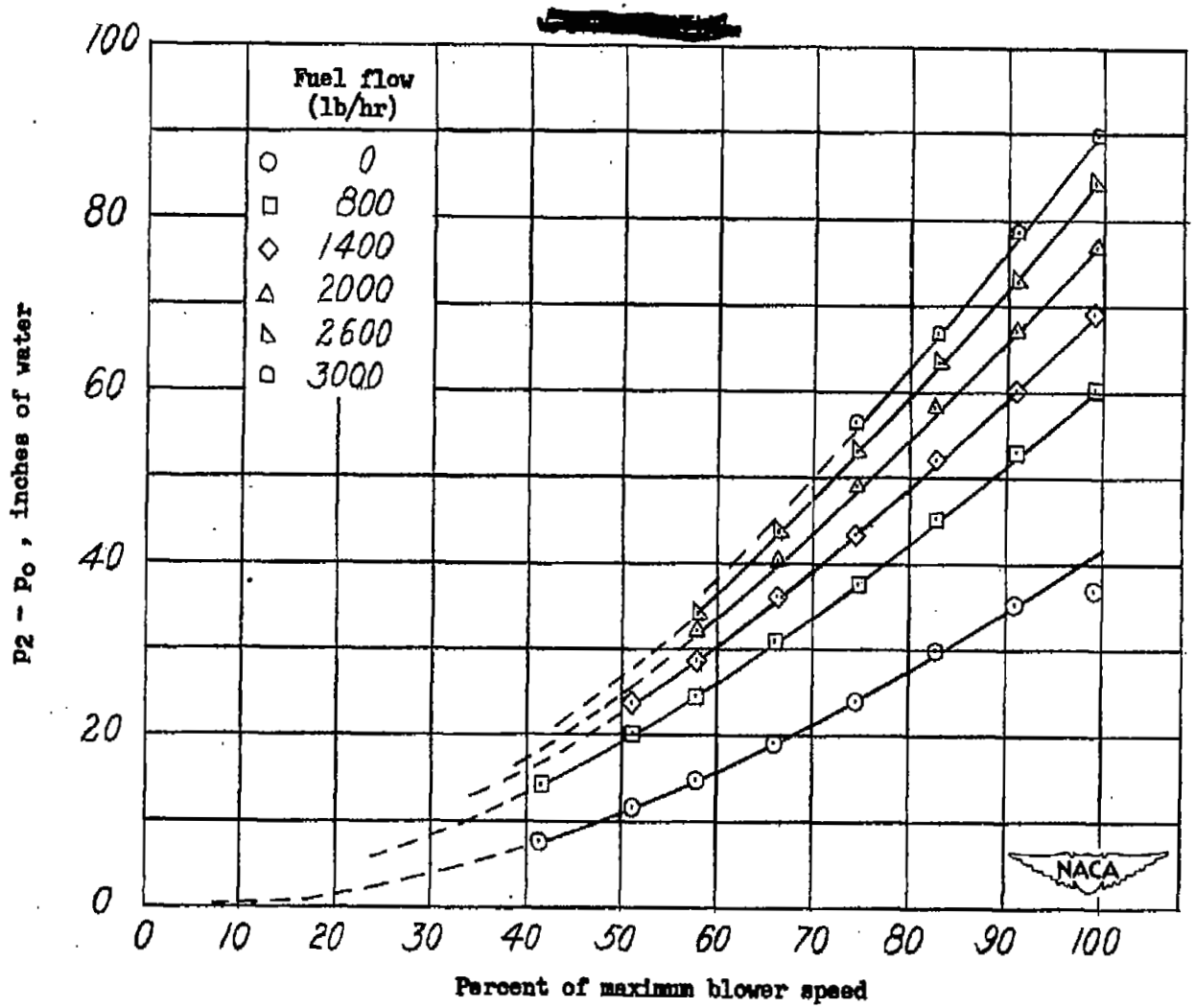

(a) $(p_2 - p_o)$ plotted against percent of maximum blower speed.

Figure 9.– Plot of average static pressure at diffuser exit.

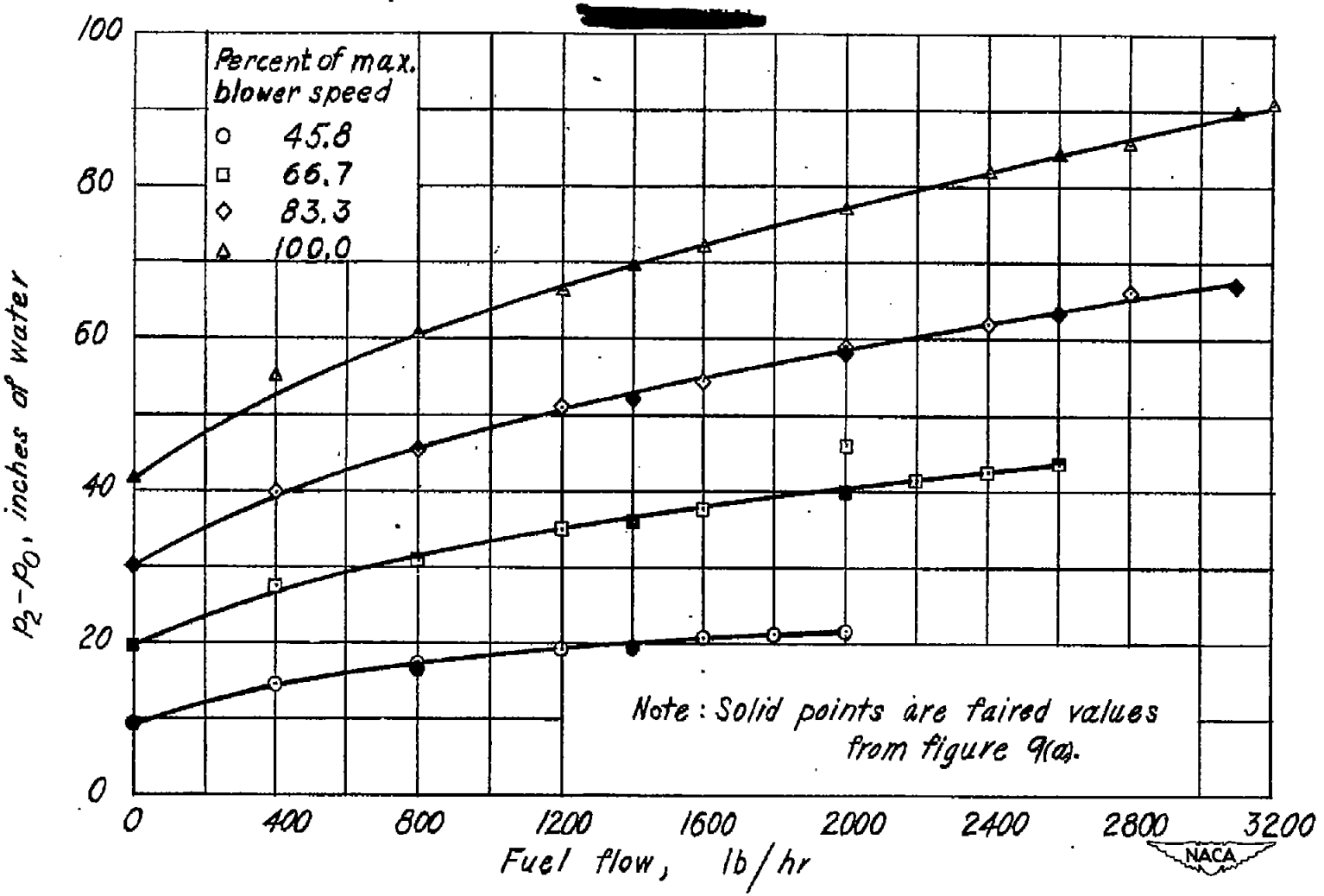

(b) $(p_2 - p_o)$ plotted against fuel flow.

Figure 9.– Concluded.

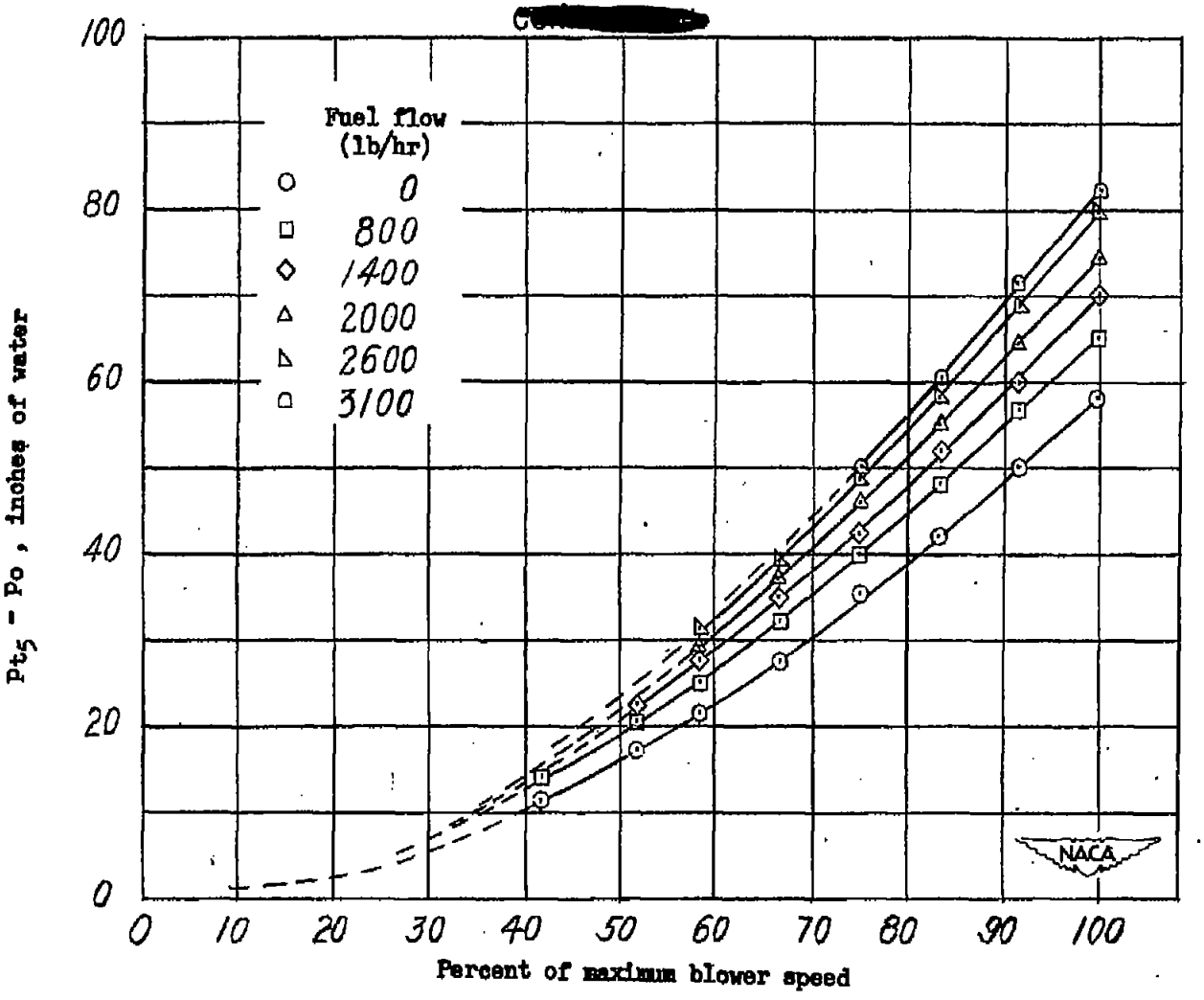

(a) $(p_{t_5} - p_o)$ plotted against percent of maximum blower speed.

Figure 10.– Plot of average total pressure at exhaust nozzle exit.

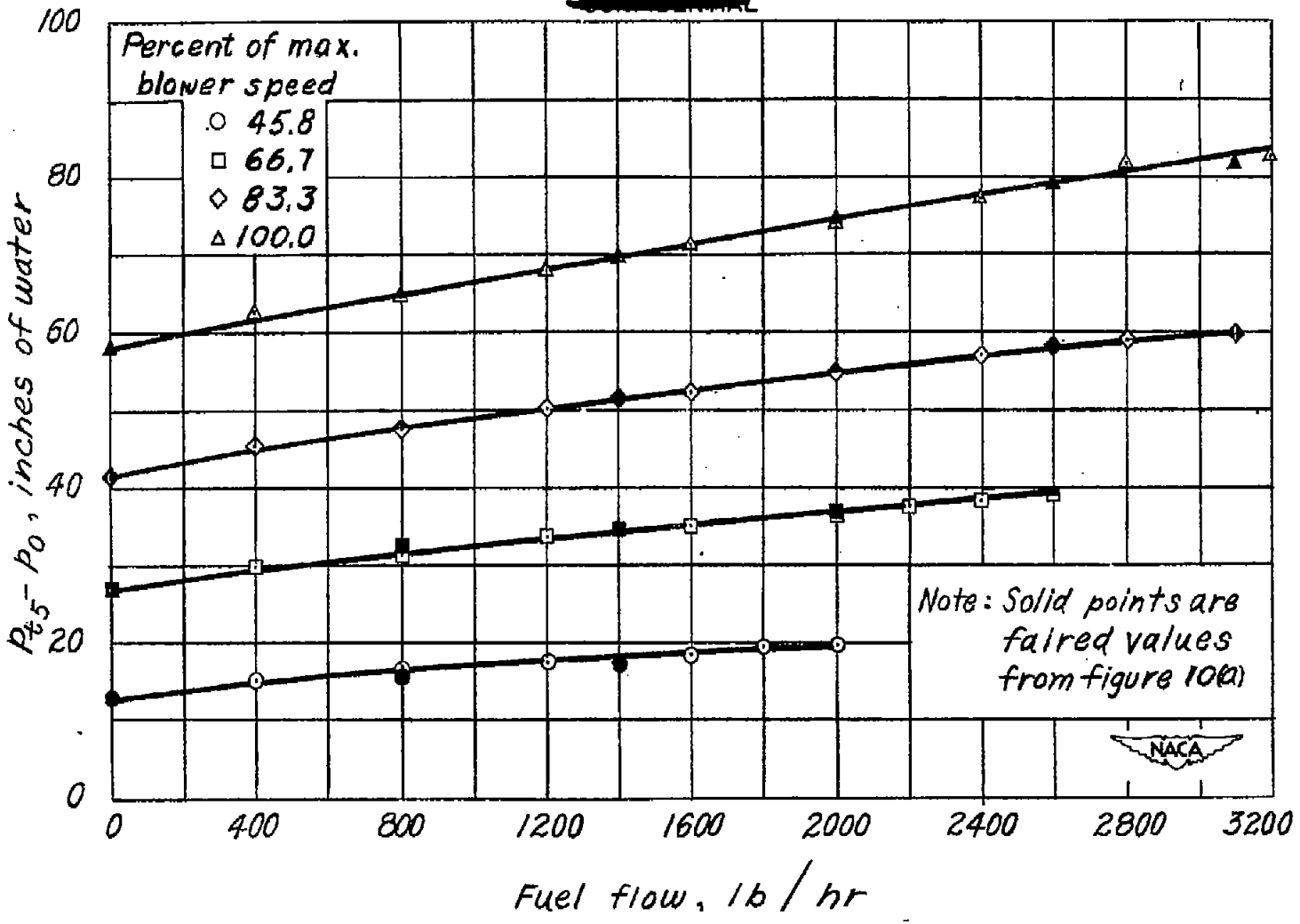

(b) $(p_{t_5} - p_0)$ plotted against fuel flow.

Figure 10.– Concluded.

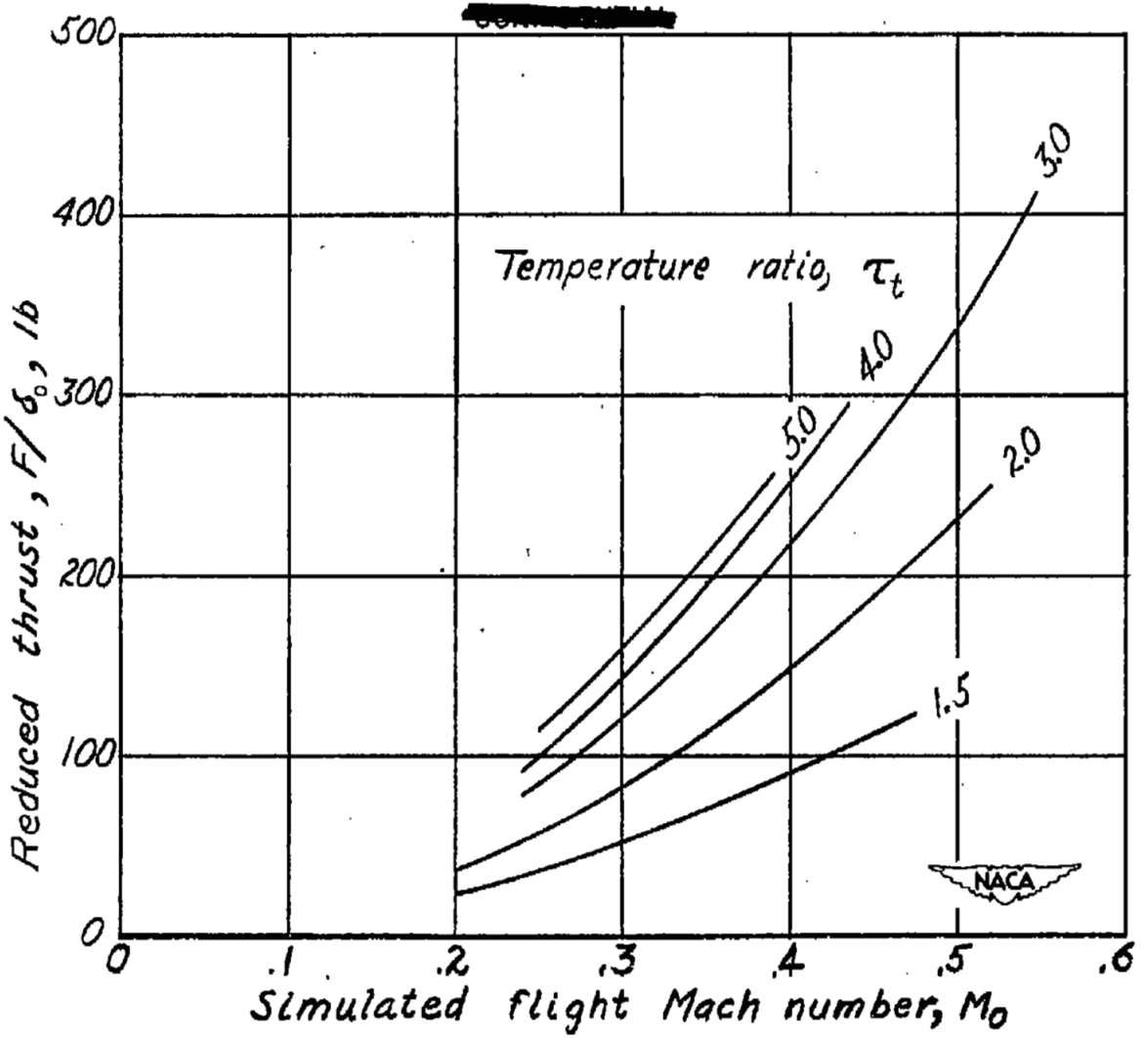

Figure 11.- Relation of reduced thrust to simulated flight Mach number for values of constant temperature ratio.

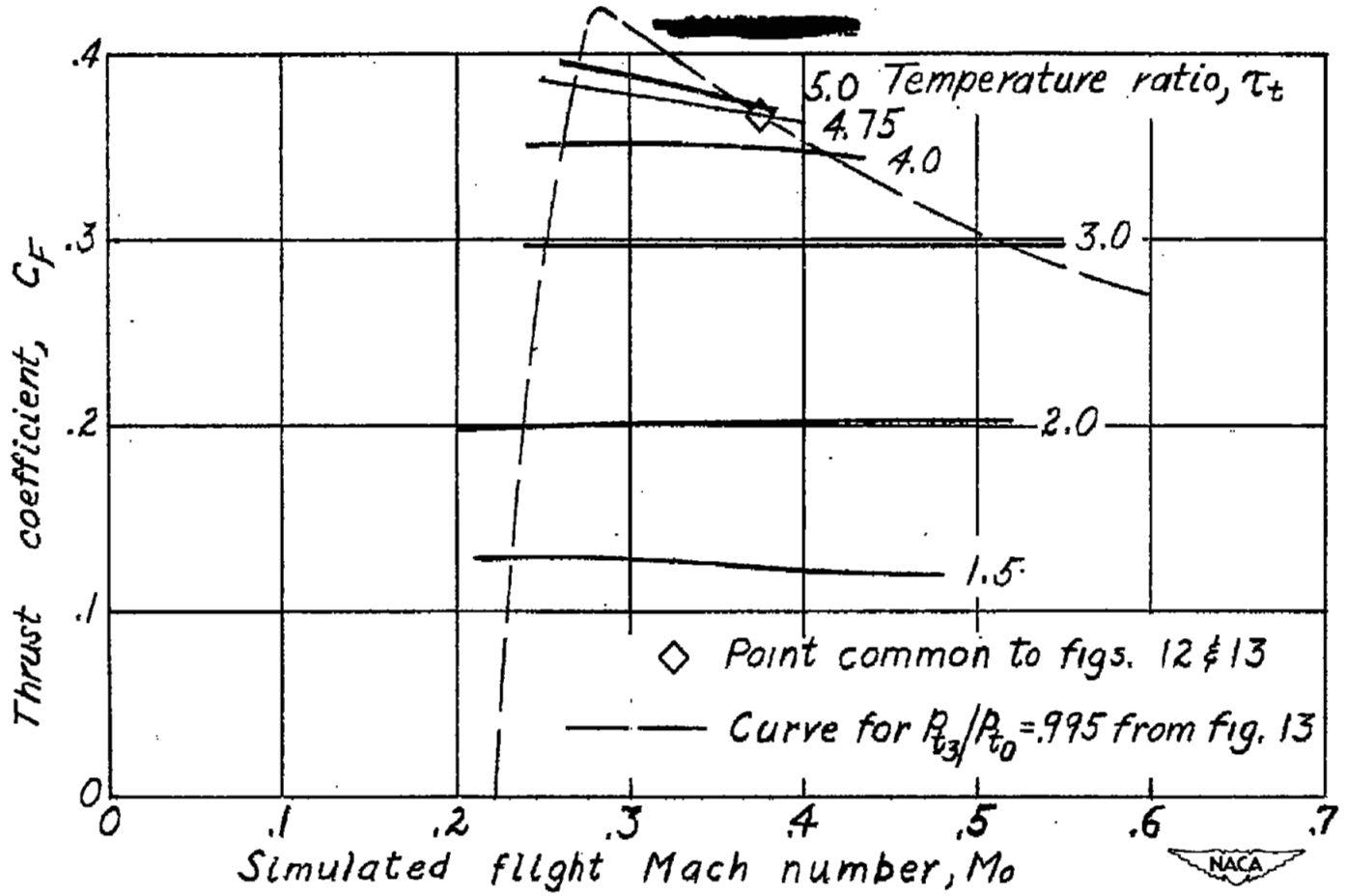

Figure 12.– Relation of thrust coefficient to simulated flight Mach number for values of constant temperature ratio, with fixed nozzle exit area and variable M_3.

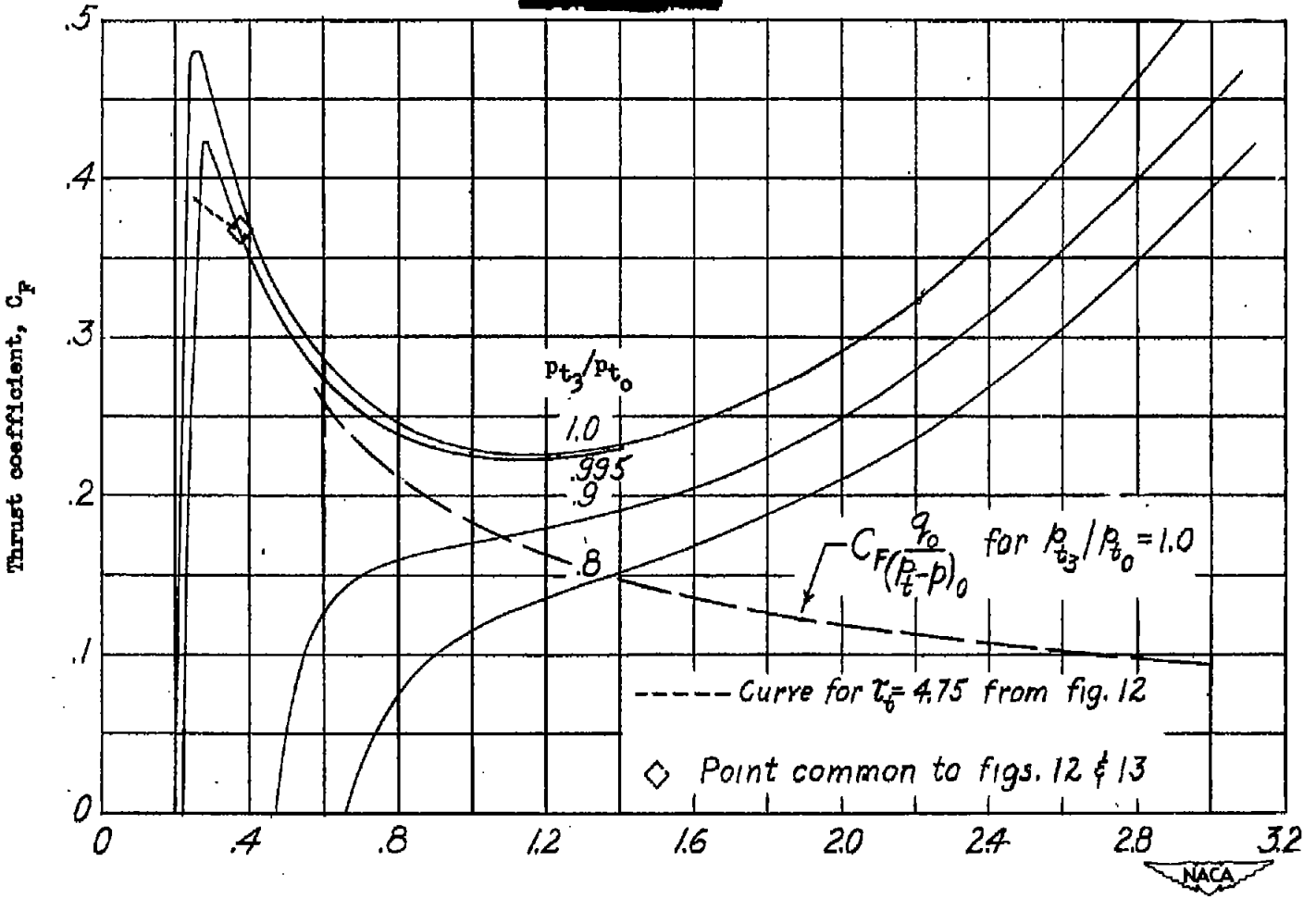

Figure 13.– Variation of C_F with M_o and p_{t_3}/p_{t_o} for $\frac{T_{t_4} - T_{t_3}}{T_o} = 3.85$, $M_3 = 0.065$, and variable nozzle exit area.

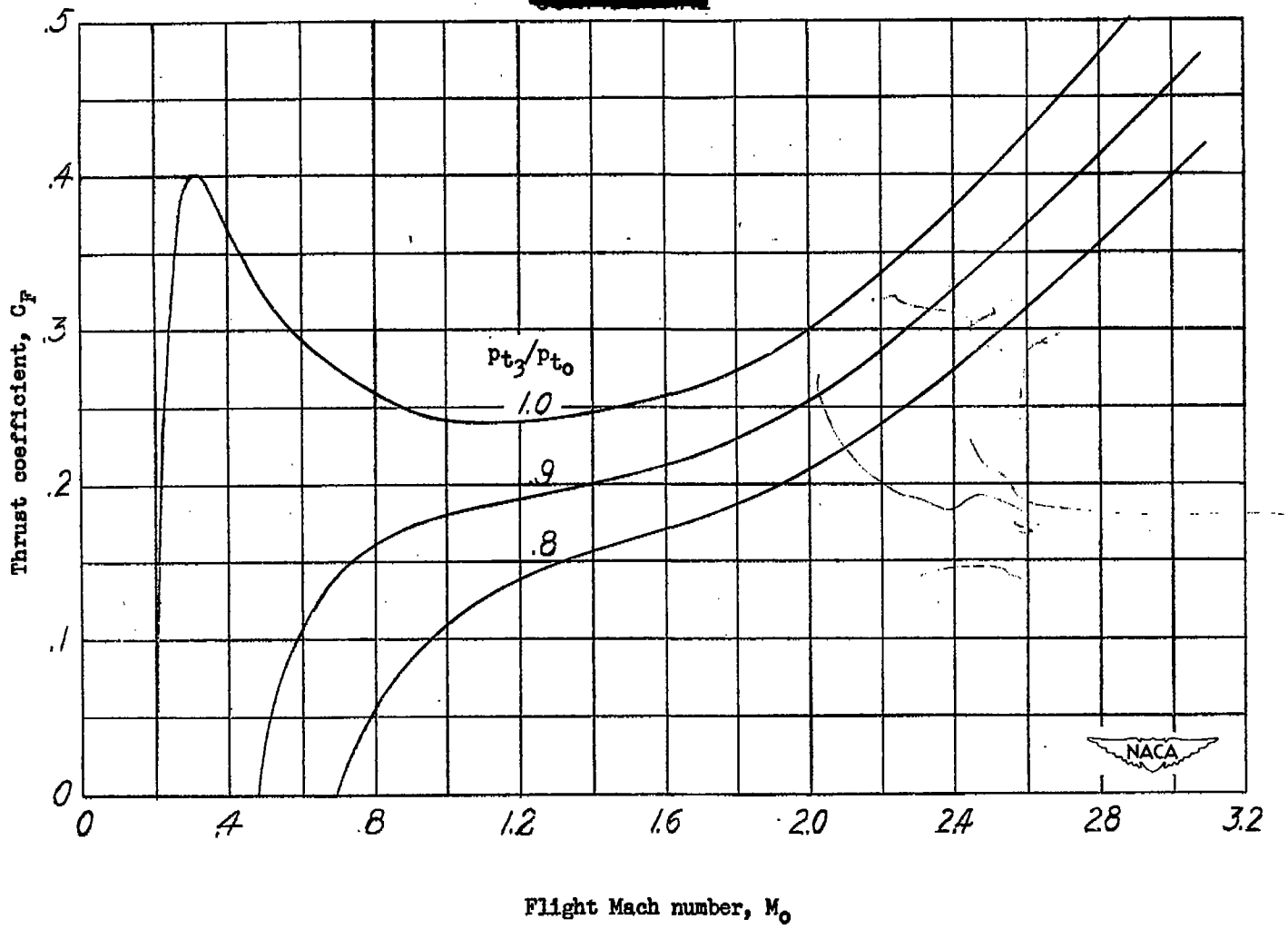

Figure 14.- Variation of C_F with M_o and p_{t_3}/p_{t_o} for $\frac{T_{t_4} - T_{t_3}}{T_o} = 2.89$, $M_3 = 0.085$, and variable nozzle exit area.

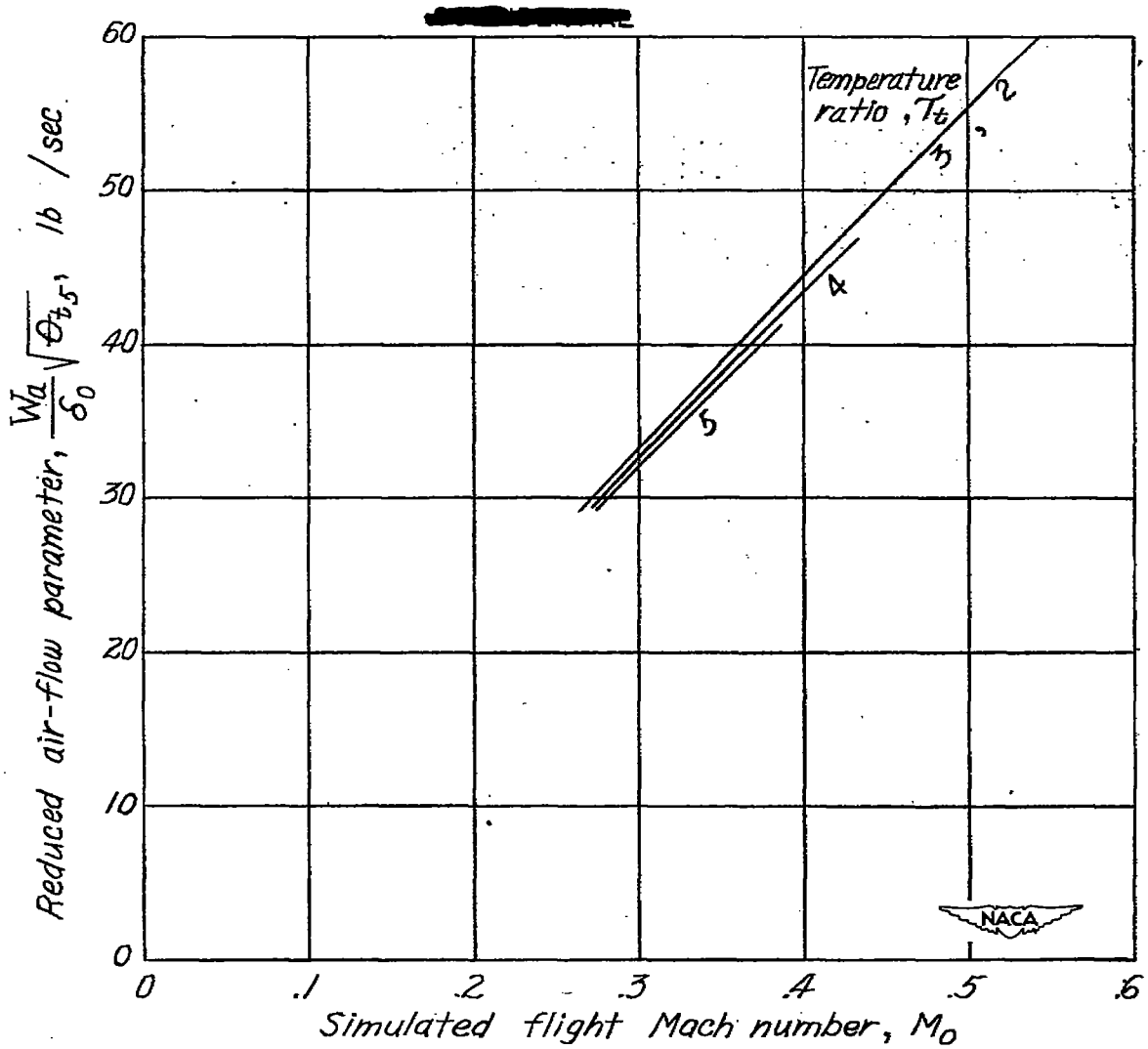

Figure 15.— Relation of reduced air-flow parameter to simulated flight Mach number.

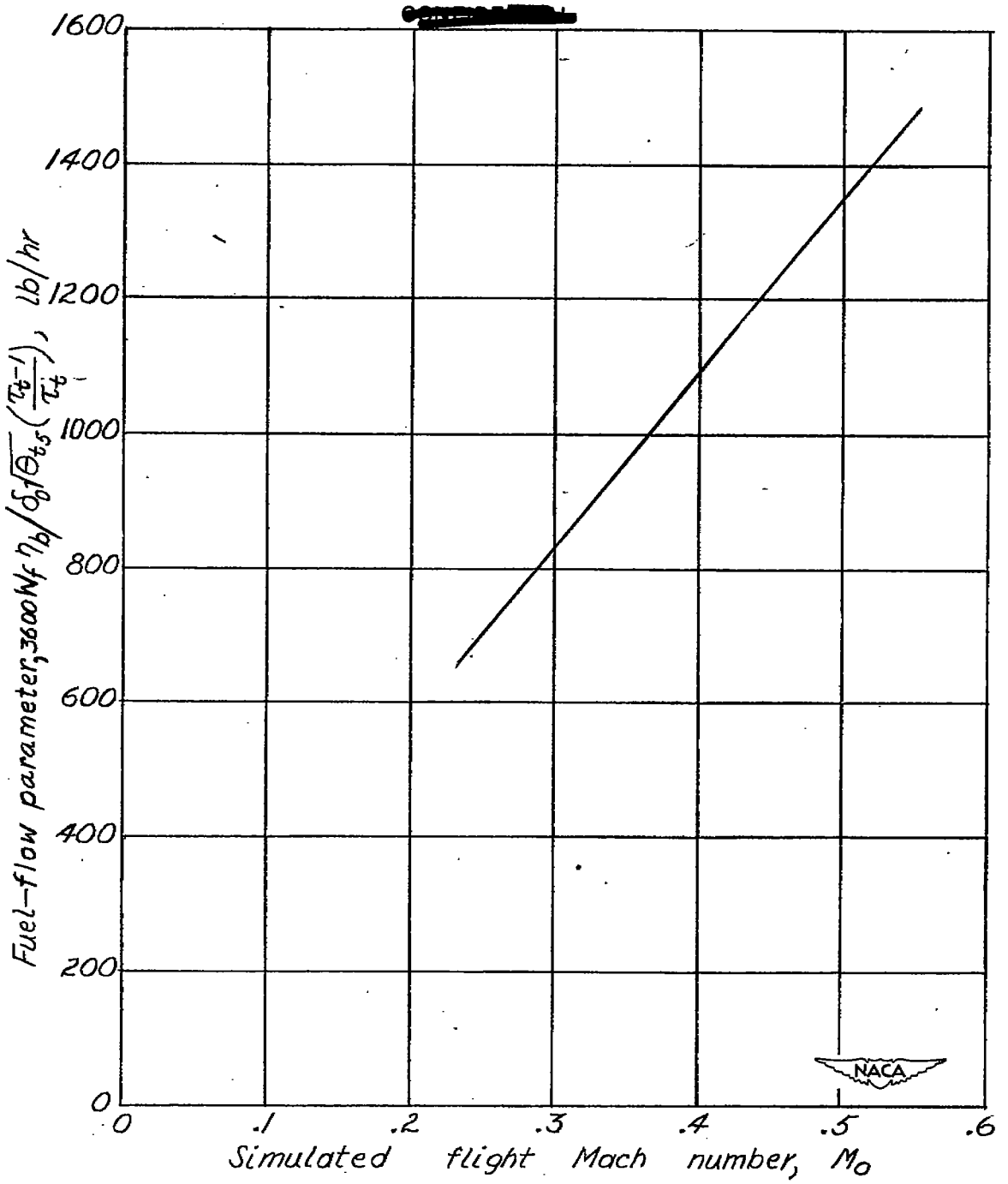

Figure 16.– Variation of fuel–flow parameter with simulated flight Mach number.

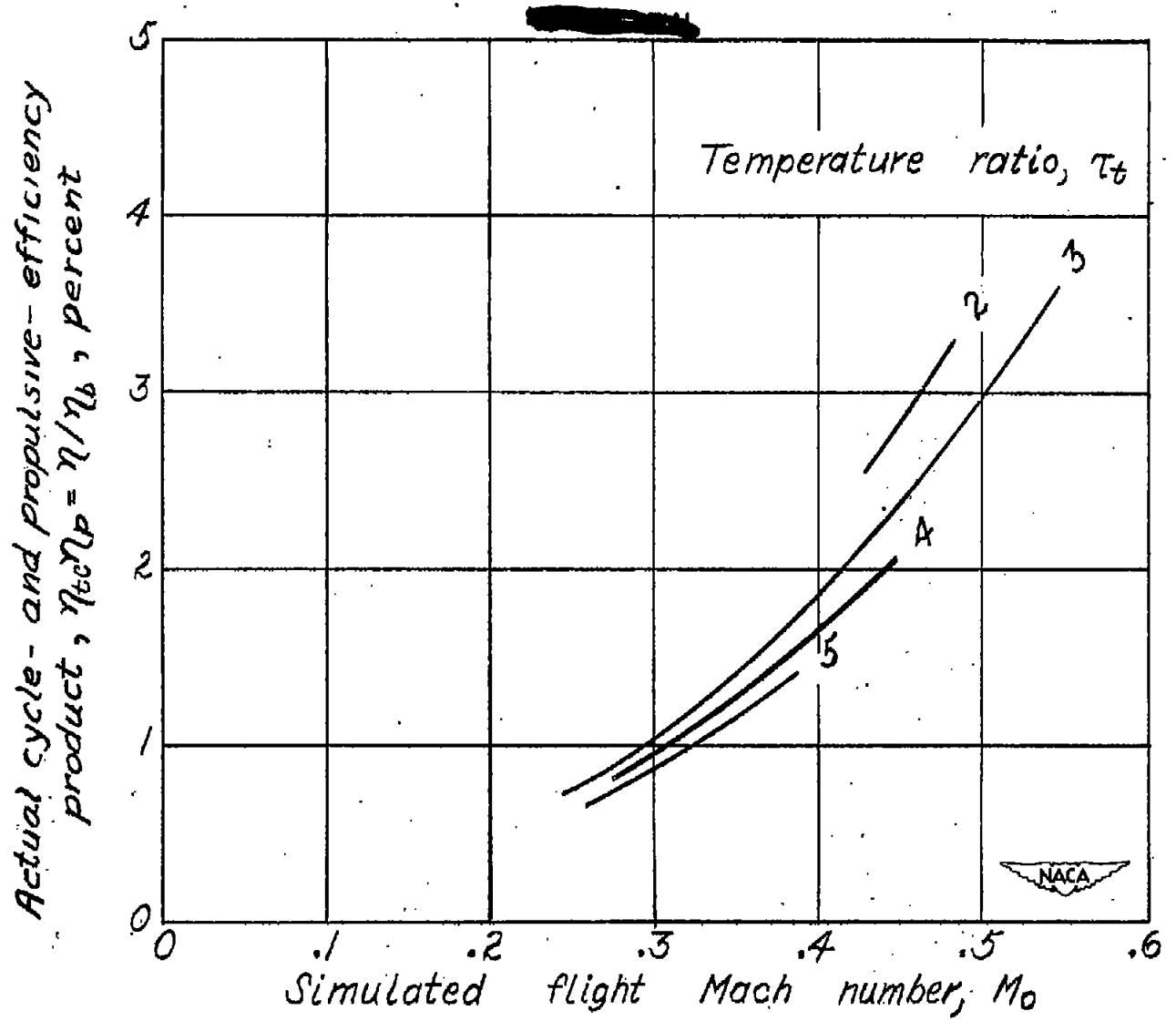

Figure 17.- Relation of actual cycle-efficiency and propulsive-efficiency product to simulated flight Mach number.

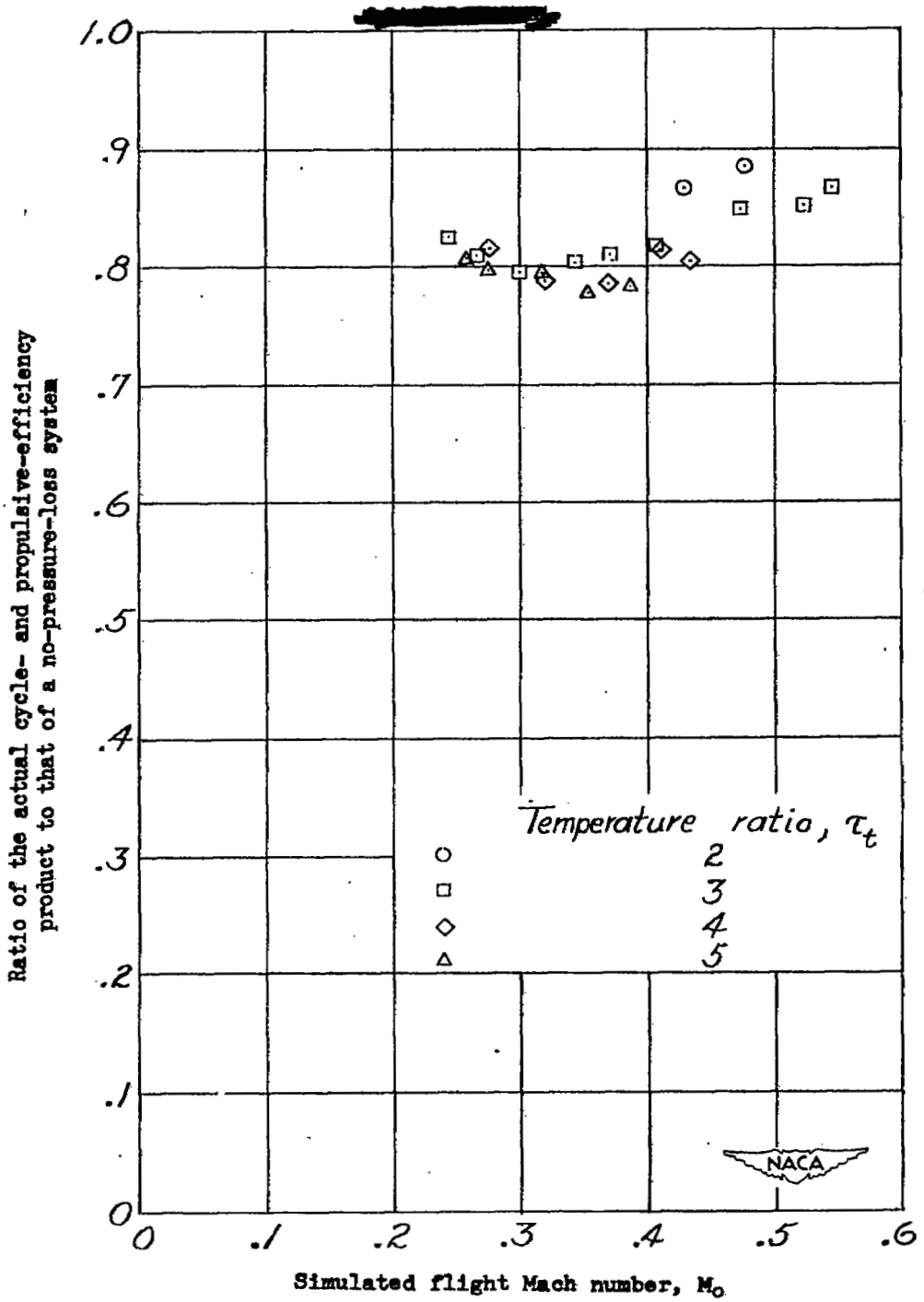

Figure 18.– Relation to simulated flight Mach number of the ratio of the actual cycle–efficiency and propulsive–efficiency product to that of a no–pressure–loss system.

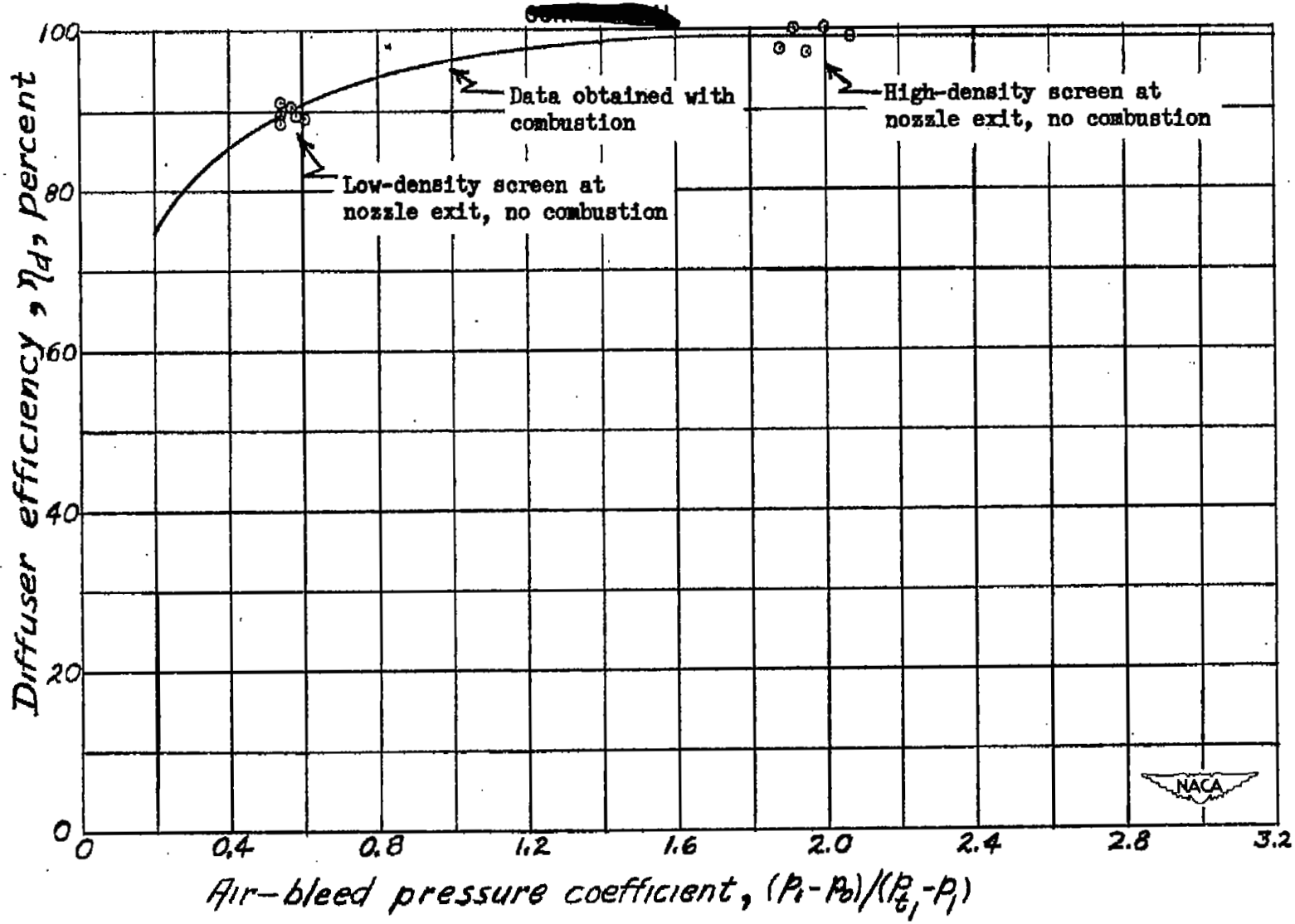

Figure 19.- Comparison of diffuser performance with and without combustion.

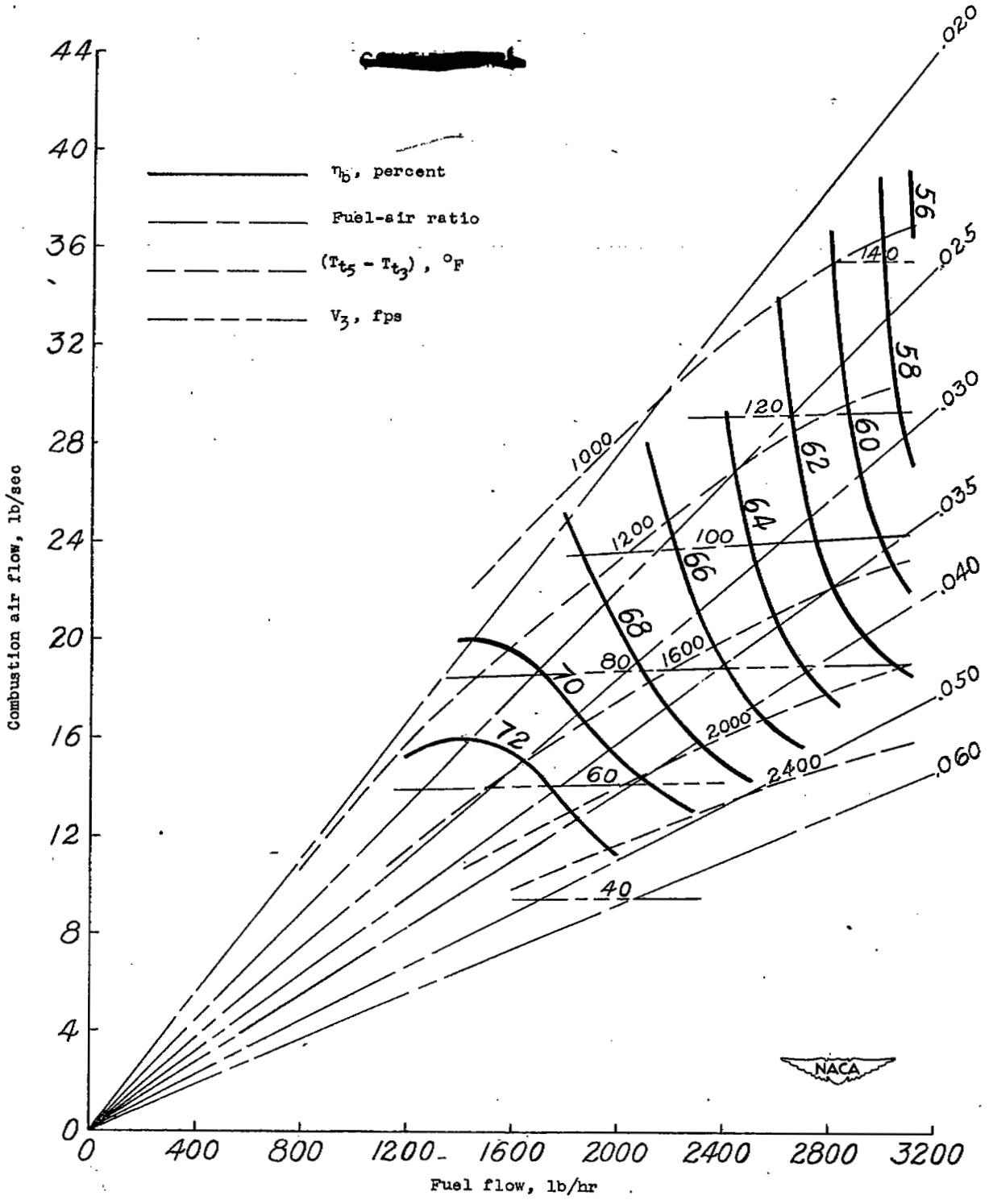

Figure 20.— Relation of combustion efficiency η_b to fuel and air flow with superimposed curves of constant fuel-air ratio, combustion temperature rise $(T_{t_5} - T_{t_3})$, and combustion-chamber inlet velocity V_3. Region covered by η_b curves represents limits of test data.

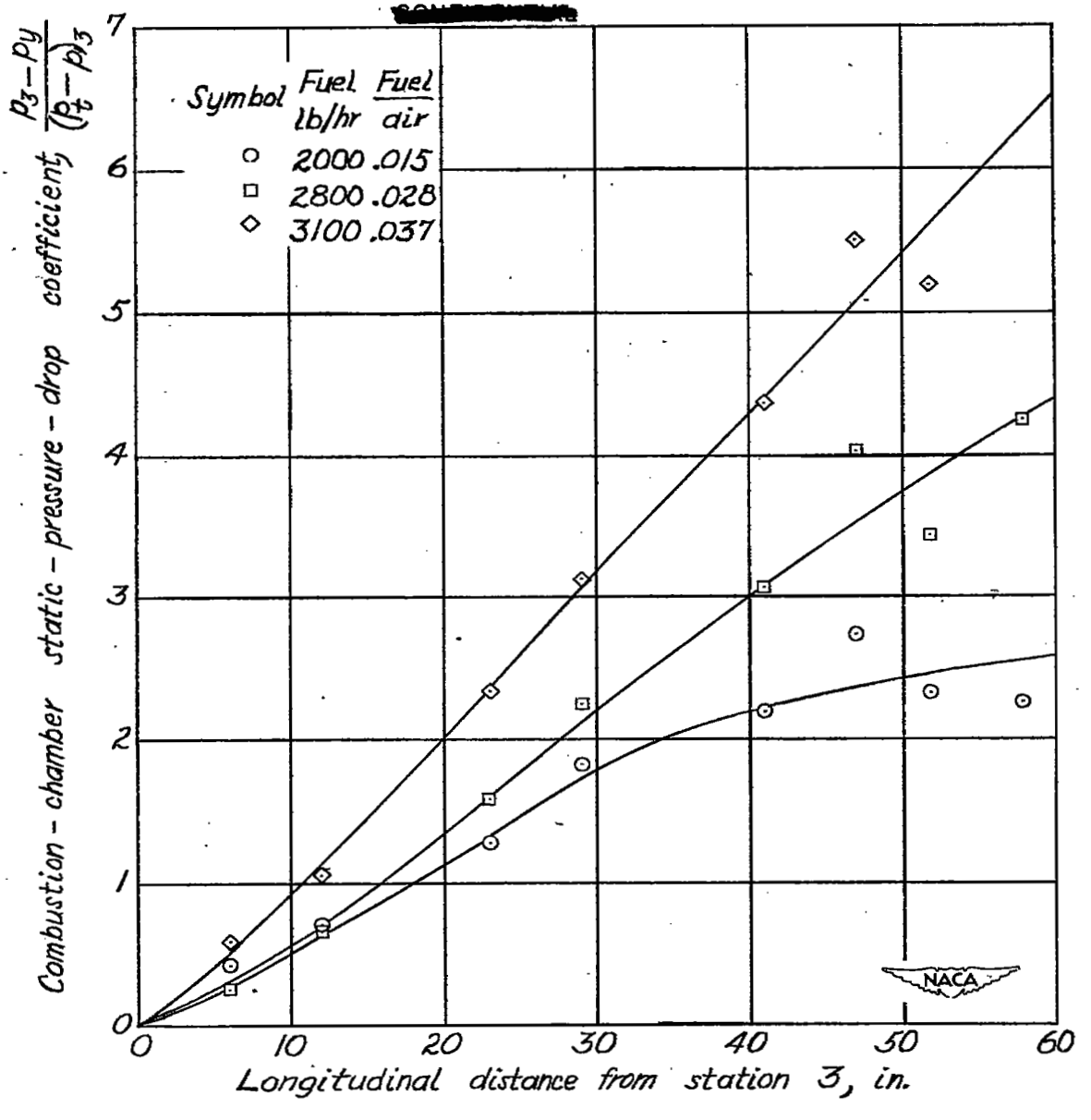

Figure 21.– Combustion–chamber longitudinal–wall static–pressure variations.

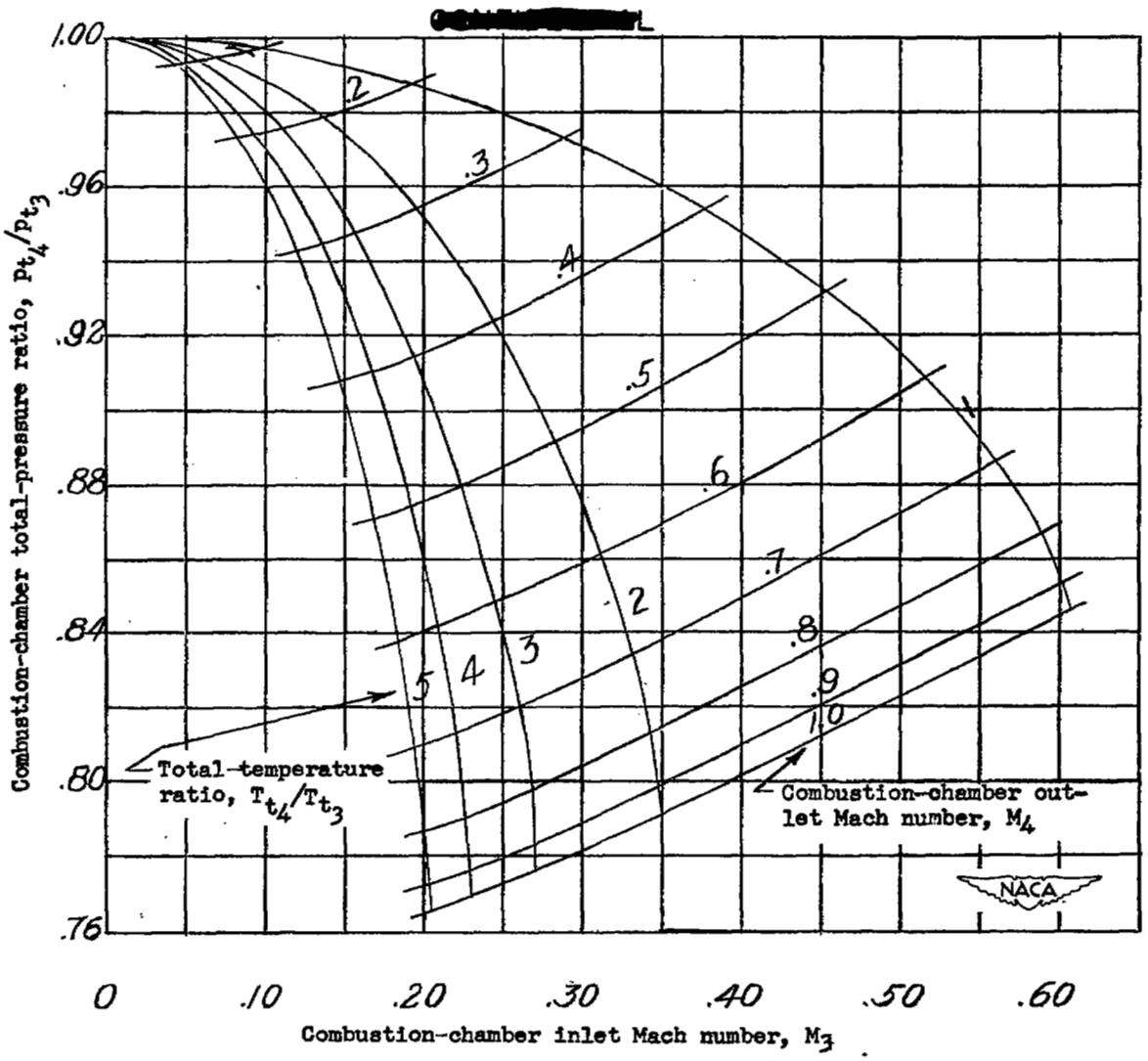

Figure 22.- Hypothetical combustion-chamber characteristics for $K_3 = 0.27$ and $K_4 = 0.18$.

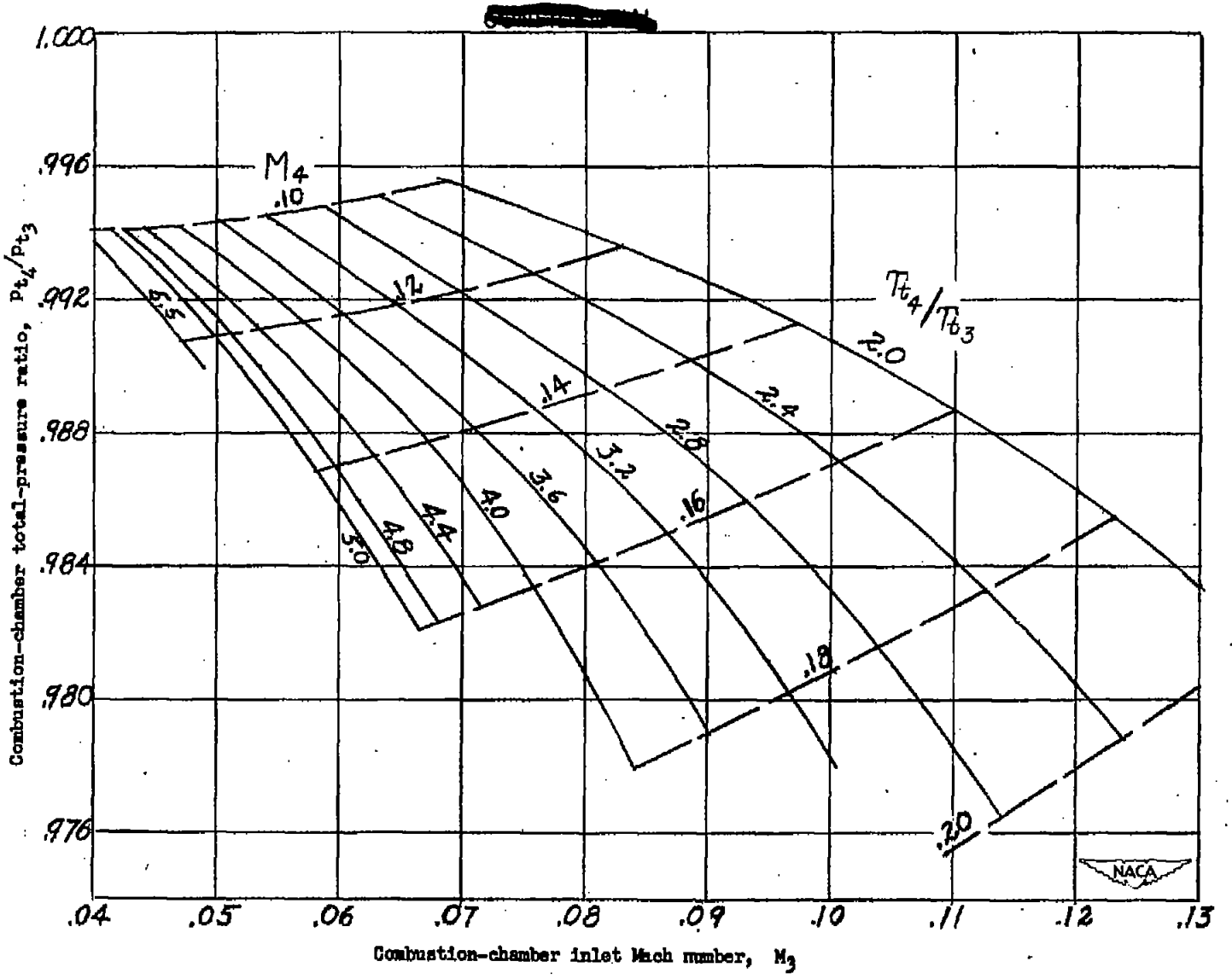

Figure 23.- Test combustion-chamber characteristics.

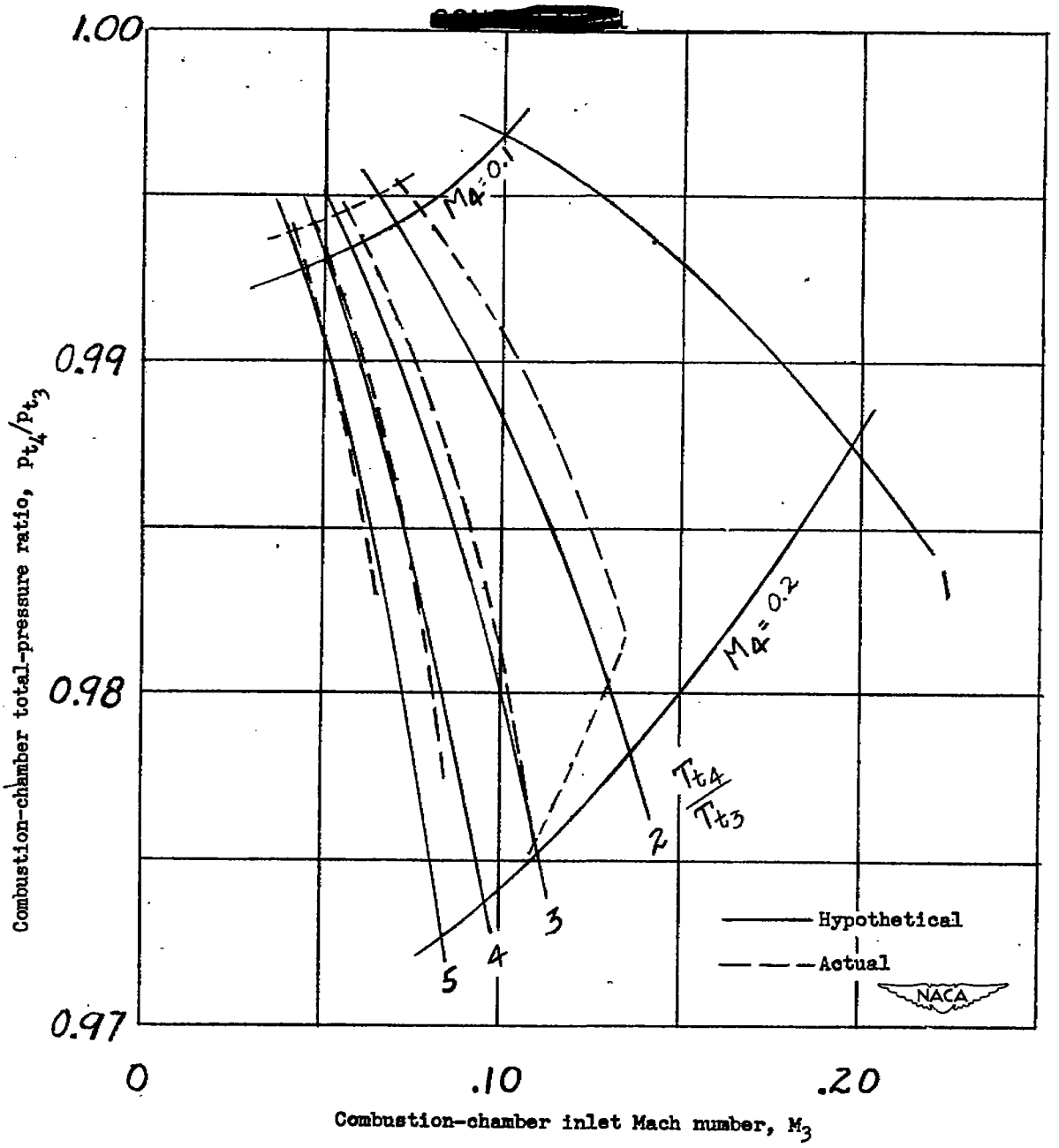

Figure 24.- Comparison of hypothetical and test combustion-chamber characteristics.

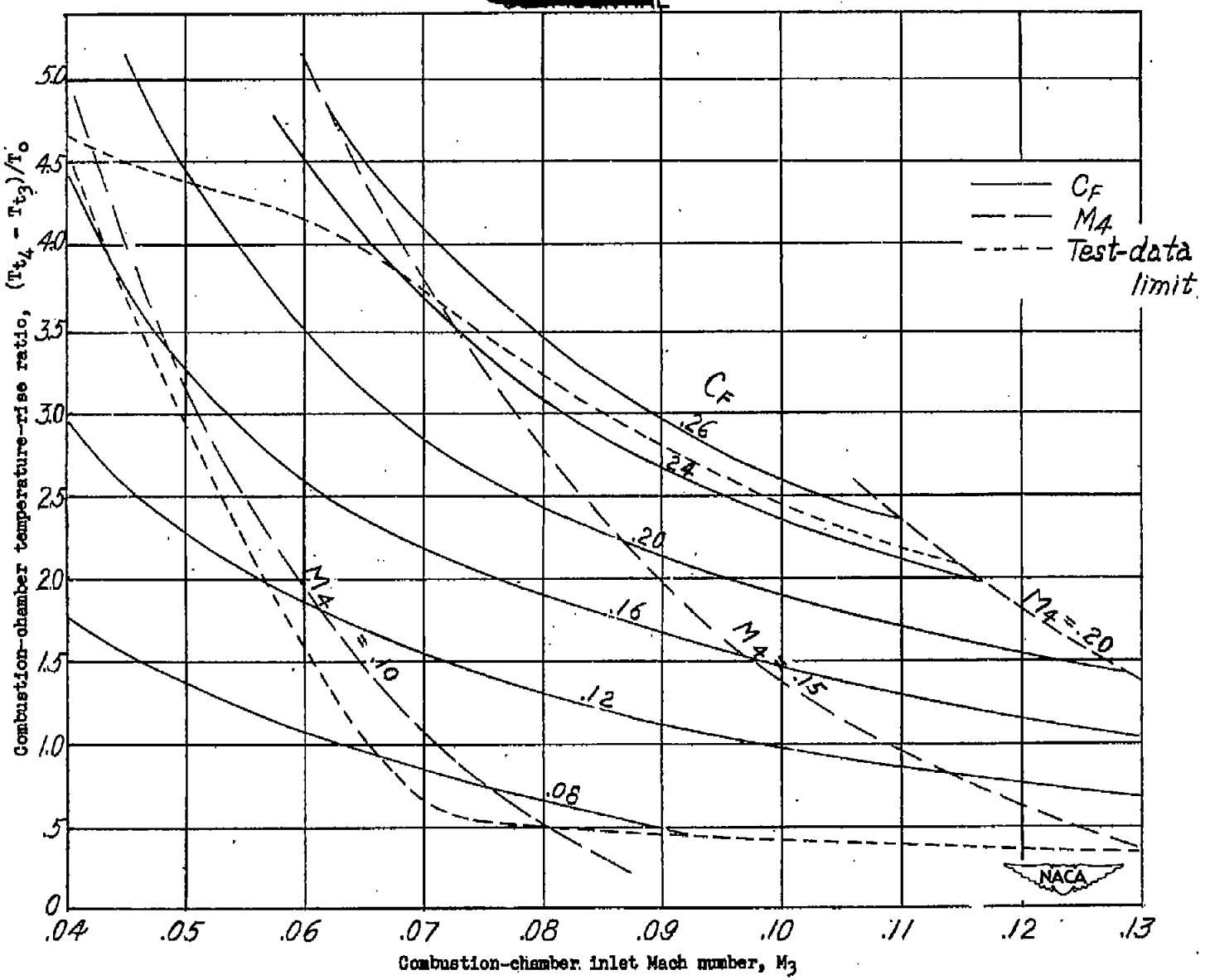

Figure 25.– Calculated thrust coefficients. $M_o = 1.0$; $\frac{Pt_3}{Pt_o} = 1.0$.

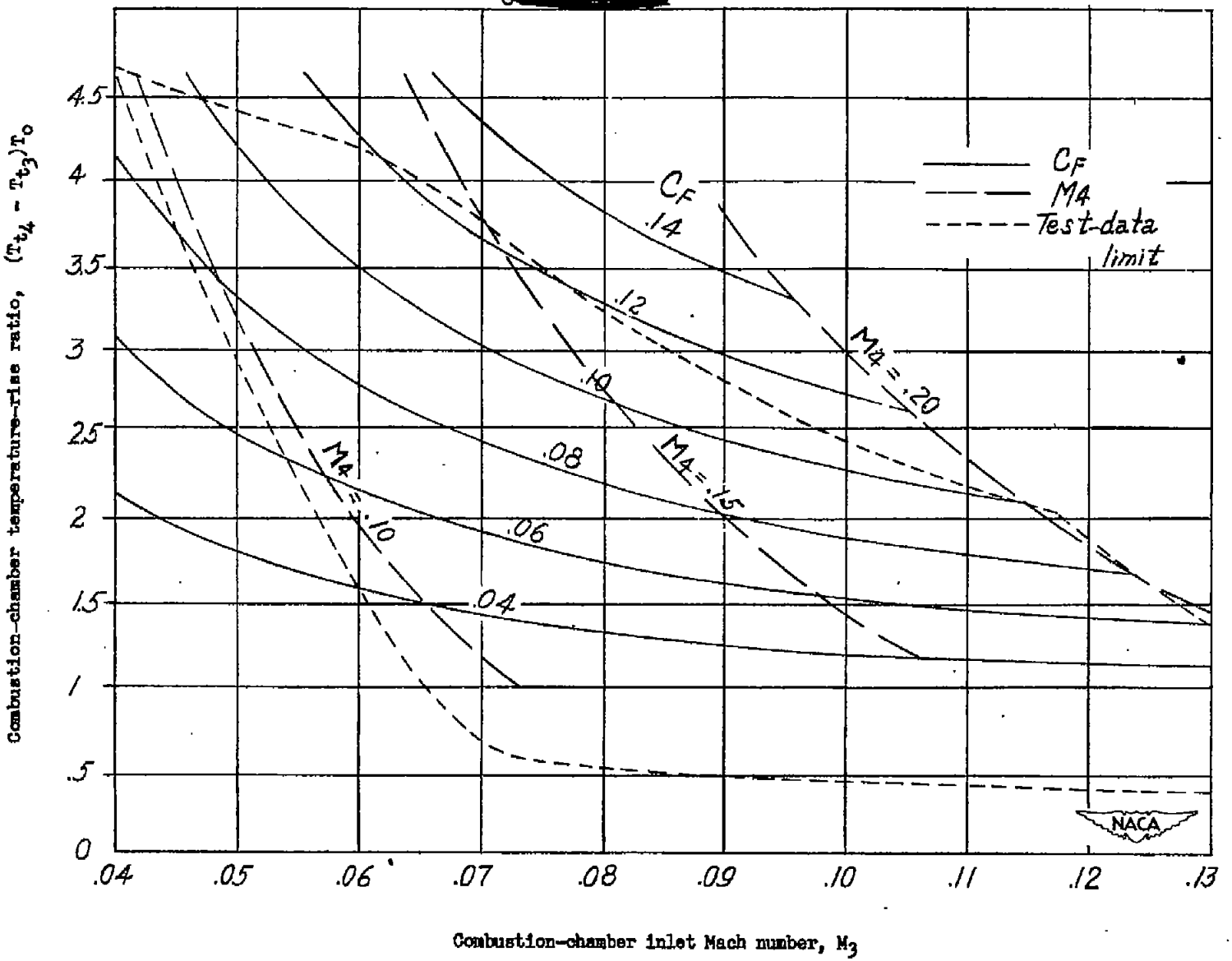

Figure 26.– Calculated thrust coefficients. $M_o = 1.0$; $\frac{p_{t_3}}{p_{t_o}} = 0.8$.

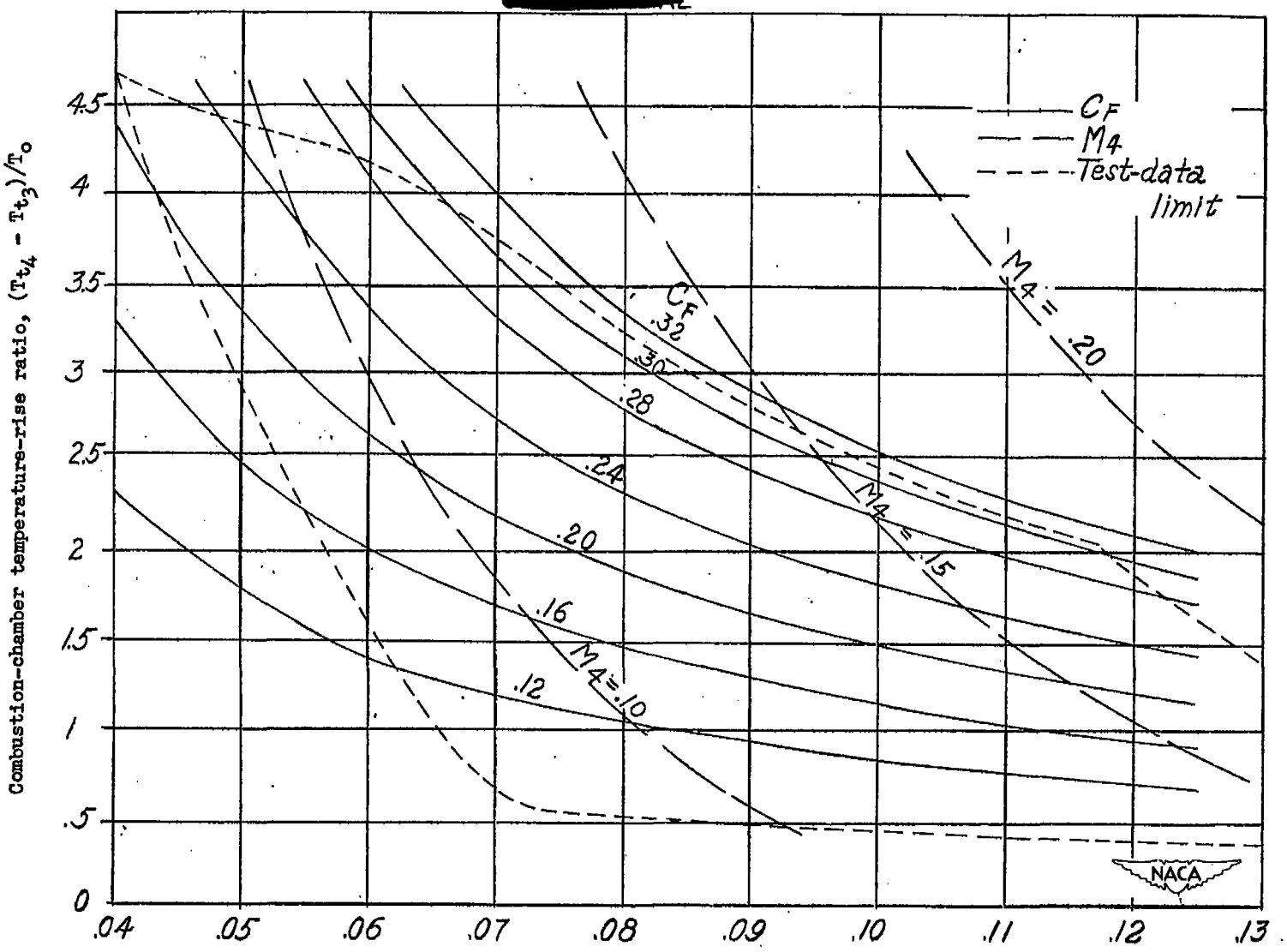

Figure 27.– Calculated thrust coefficient. $M_o = 2.0$; $\frac{p_{t_3}}{p_{t_o}} = 1.0$.

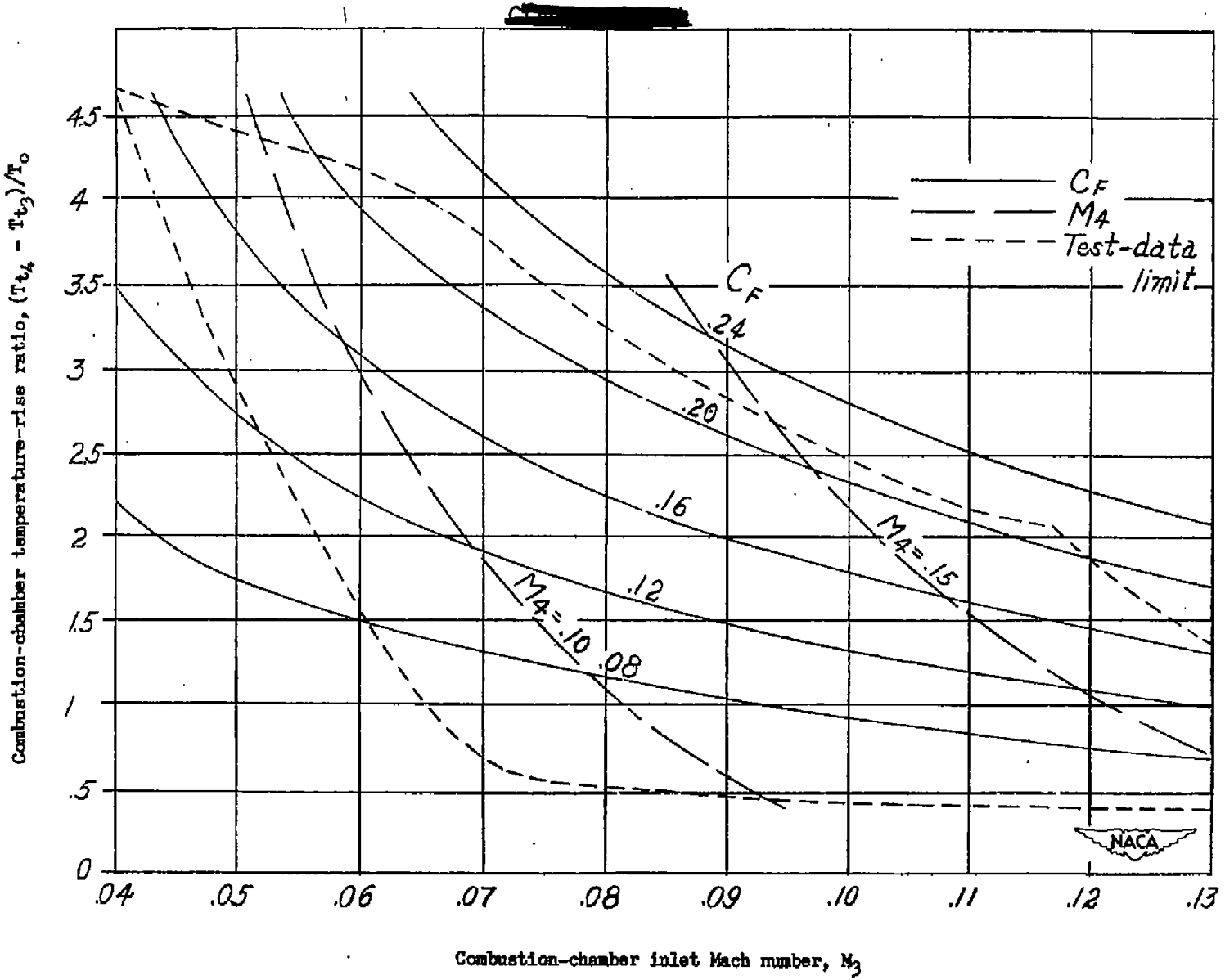

Figure 28.– Calculated thrust coefficients. $M_o = 2.0$; $\frac{p_{t_3}}{p_{t_o}} = 0.8$.